

SOURCE
DATATRANSPARENT
PROCESSOPEN
ACCESS

SCF (Fbx17) ubiquitylation of Sufu regulates Hedgehog signaling and medulloblastoma development

Madalina Raducu¹, Ella Fung¹, Sébastien Serres¹, Paola Infante², Alessandro Barberis¹, Roman Fischer³, Claire Bristow¹, Marie-Laëtitia Thézénas³, Csaba Finta⁴, John C Christianson⁵, Francesca M Buffa¹, Benedikt M Kessler³, Nicola R Sibson¹, Lucia Di Marcotullio^{6,7}, Rune Toftgård⁴ & Vincenzo D'Angiolella^{1,*}

Abstract

Skp1-Cul1-F-box protein (SCF) ubiquitin ligases direct cell survival decisions by controlling protein ubiquitylation and degradation. Sufu (Suppressor of fused) is a central regulator of Hh (Hedgehog) signaling and acts as a tumor suppressor by maintaining the Gli (Glioma-associated oncogene homolog) transcription factors inactive. Although Sufu has a pivotal role in Hh signaling, the players involved in controlling Sufu levels and their role in tumor growth are unknown. Here, we show that Fbx17 (F-box and leucine-rich repeat protein 17) targets Sufu for proteolysis in the nucleus. The ubiquitylation of Sufu, mediated by Fbx17, allows the release of Gli1 from Sufu for proper Hh signal transduction. Depletion of Fbx17 leads to defective Hh signaling associated with an impaired cancer cell proliferation and medulloblastoma tumor growth. Furthermore, we identify a mutation in Sufu, occurring in medulloblastoma of patients with Gorlin syndrome, which increases Sufu turnover through Fbx17-mediated polyubiquitylation and leads to a sustained Hh signaling activation. In summary, our findings reveal Fbx17 as a novel regulator of Hh pathway and highlight the perturbation of the Fbx17–Sufu axis in the pathogenesis of medulloblastoma.

Keywords F-box protein; Fbx17; Hedgehog signaling; medulloblastoma; Sufu

Subject Categories Cancer; Post-translational Modifications, Proteolysis & Proteomics; Signal Transduction

DOI 10.15252/emboj.201593374 | Received 28 October 2015 | Revised 28 April 2016 | Accepted 29 April 2016 | Published online 27 May 2016

The EMBO Journal (2016) 35: 1400–1416

Introduction

Signals of the Hh (Hedgehog) pathway are essential in directing cell proliferation and patterning during embryogenesis (Hooper & Scott, 2005; Ingham *et al.*, 2011). The pathway lays at the cross-road of cell survival and differentiation decisions, and unscheduled Hh signaling can lead to hyperproliferation and the development of malignancies. Indeed, alterations of pathway components have been described in multiple cancer types (Teglund & Toftgård, 2010).

Hh signaling is initiated at the cell membrane by the inactivation of the 12-pass transmembrane receptor Ptch (Patched) upon binding of the Hh ligands (Ingham *et al.*, 2011). Ptch inactivation frees the cognate receptor Smo (Smoothed) leading to the downstream activation of a transcriptional program mediated by Gli1, Gli2, and Gli3 (Glioma-associated oncogene homolog 1, 2, and 3) transcription factors (Hui & Angers, 2011).

Sufu (Suppressor of fused) acts as a central negative regulator of Hh signaling by sequestering the Gli transcription factors in an inactive complex (Kogerman *et al.*, 1999; Dunaeva *et al.*, 2003; Merchant *et al.*, 2004; Humke *et al.*, 2010). Sufu deletion in mice leads to the continuous activation of Hh signal and embryonic lethality at day 9.5 (Cooper *et al.*, 2005; Svard *et al.*, 2006), underscoring the essential role of Sufu for proper development. Importantly, heterozygous loss of Sufu, in conjunction with the loss of p53, leads to the development of medulloblastoma and rhabdomyosarcoma (Lee *et al.*, 2007). Germline Sufu mutations have been identified in medulloblastoma (Taylor *et al.*, 2002; Kool *et al.*, 2014) and associated with the development of medulloblastoma in Gorlin syndrome (Pastorino *et al.*, 2009; Kijima *et al.*, 2012; Smith *et al.*, 2014). Furthermore, somatic Sufu mutations have been identified in multiple other malignancies, including prostate cancer (Sheng *et al.*, 2004).

1 Cancer Research UK and Medical Research Council Institute for Radiation Oncology, Department of Oncology, University of Oxford, Oxford, UK

2 Center for Life NanoScience@Sapienza, Istituto Italiano di Tecnologia, Rome, Italy

3 Target Discovery Institute, Nuffield Department of Medicine, University of Oxford, Oxford, UK

4 Department of Biosciences and Nutrition, Center for Innovative Medicine, Karolinska Institutet, Huddinge, Sweden

5 Ludwig Institute for Cancer Research, University of Oxford, Oxford, UK

6 Department of Molecular Medicine, University “La Sapienza”, Rome, Italy

7 Pasteur Institute/Cenci Bolognetti Foundation, Sapienza University, Rome, Italy

*Corresponding author. Tel: +44 01865617400; E-mail: vincenzo.dangiolella@oncology.ox.ac.uk

Sufu has a pivotal role in Hh signaling and is a relevant tumor suppressor, but the players involved in controlling Sufu levels are unknown and the relevance for cancer proliferation remains unrecognized.

Using an unbiased proteomic approach, we have identified Sufu as an interacting partner of the E3 ubiquitin ligase Fbx17 (F-box and leucine-rich repeat protein 17). Fbx17 belongs to a family of E3 ubiquitin ligases containing a leucine-rich repeat and an F-box motif, which mediate binding to Skp1 (S-phase kinase-associated protein 1) (Skaar *et al*, 2009). Skp1 in turn recruits Cul1 (Cullin 1) and Rbx1 (RING-box protein 1) for the formation of an SCF (Skp1-Cul1-F-box protein) complex. The multi-subunit SCF directs the polyubiquitylation of target substrates by recruiting an E2 enzyme with an activated ubiquitin molecule ready to be transferred on accepting lysines of target substrates. Substrate specificity is dictated by the presence of variable protein–protein interaction domains within diverse F-box proteins (Skaar *et al*, 2013). According to the type of protein–protein interaction domain, three subfamilies of F-box proteins have been identified in the human genome: Fbxws (containing WD40 repeats), Fbxls (containing leucine-rich repeats, LRR), and Fbxos (containing other interacting motifs) (Jin *et al*, 2004).

F-box proteins can function as tumor suppressor or oncogenes and have been implicated in the control of cell proliferation and cancer development (D'Angiolella *et al*, 2012; Bassermann *et al*, 2014). Novel compounds targeting F-box proteins have been developed, and therefore, F-box proteins represent candidate pharmacological targets to treat cancer (Skaar *et al*, 2014). However, few F-box proteins have been matched to substrates and biological roles.

Here, we show that Fbx17 forms a functional SCF complex and targets the tumor suppressor Sufu for proteolysis in the nuclear compartment upon Hh pathway activation. The ubiquitylation of

Sufu, mediated by Fbx17, allows the release of Gli1 for full activation of the Hh signaling. Extending our basic biological finding to the significance of the Fbx17–Sufu axis *in vivo*, we have identified Fbx17 as a crucial regulator of cell proliferation in medulloblastoma.

Finally, we show that in human disease, a somatic mutation in Sufu, occurring in medulloblastoma of patients with Gorlin syndrome, increases Sufu turnover through Fbx17 polyubiquitylation, leading to a sustained Hh signaling and cell proliferation. Our study highlights the alteration in Fbx17–Sufu axis as an etiological mechanism of medulloblastoma.

Results

Fbx17 interacts with Sufu and regulates Sufu levels

To identify the putative functions and substrates of Fbx17, we isolated Fbx17 and interacting proteins from HEK293T cells. Liquid chromatography–tandem mass spectrometry (LC-MS/MS) of the immunoprecipitated material identified peptides corresponding to components of the SCF complex (Skp1 and Cul1), peptides corresponding to BACH1 (BTB and CNC homology 1 protein, a known substrate of Fbx17) (Tan *et al*, 2013) as well as putative novel substrates such as Sufu and ZBTB33 (Zinc Finger and BTB domain containing 33) (Table 1).

Since a single substrate might be targeted by different ligases (like in the case of β -TrCP1 and β -TrCP2; beta-transducin repeat containing E3 ubiquitin protein ligase 1 and 2) (Guardavaccaro *et al*, 2003), we screened a panel of Flag-tagged F-box proteins isolated from HEK293T cells for the binding to Sufu. We detected Sufu only in Fbx17 co-immunoprecipitates (Fig 1A), whereas all F-box proteins bound to Skp1.

Table 1. Proteins associated with Fbx17 identified by mass spectrometry.

Accession	Score	Mass	No. matches	No. sig. matches	No. seq	No. sig. seq	emPAI	Description
Q9UF56	33,624	77,984	1,316	1,081	76	74	178.17	Fbx17
P63208	8,032	18,817	297	243	17	15	59.82	Skp1
Q13616	248	90,306	14	12	9	7	0.28	Cul1
Q9UMX1	112	54,255	9	5	3	3	0.27	Sufu
Q96DT7	102	95,975	6	3	4	3	0.11	ZBTB10
Q9BY89	79	197,617	9	4	9	4	0.07	KIAA1671
Q86T24	65	75,065	1	1	1	1	0.04	ZBTB33
O14867	59	83,844	2	1	2	1	0.04	BACH1
O43318	55	67,895	4	2	4	2	0.10	TAB 1
O43164	39	79,192	3	1	3	1	0.04	Praja2
Q04721	21	279,082	5	2	3	1	0.01	Notch 2
Q9BXU1	20	116,647	7	1	3	1	0.03	Sgk396
O14641	17	79,184	5	1	5	1	0.04	DSH homolog 2
O15355	16	59,919	9	2	6	2	0.11	PPM1G

The table represents the summary of four independent 3×Flag-tagged Fbx17 immunoprecipitation experiments followed by liquid chromatography–mass spectrometry (LC/MS). Identified interacting proteins in Fbx17 were filtered using LC/MS data from 8 independent analyses of unrelated F-box proteins 3×Flag immunoprecipitations. Results were scored according to confidence of identification and a Mascot Mowse cutoff score of 50 was established. Proteins identified with a Mascot cutoff score below 50 in more than one biological replicate are also reported.

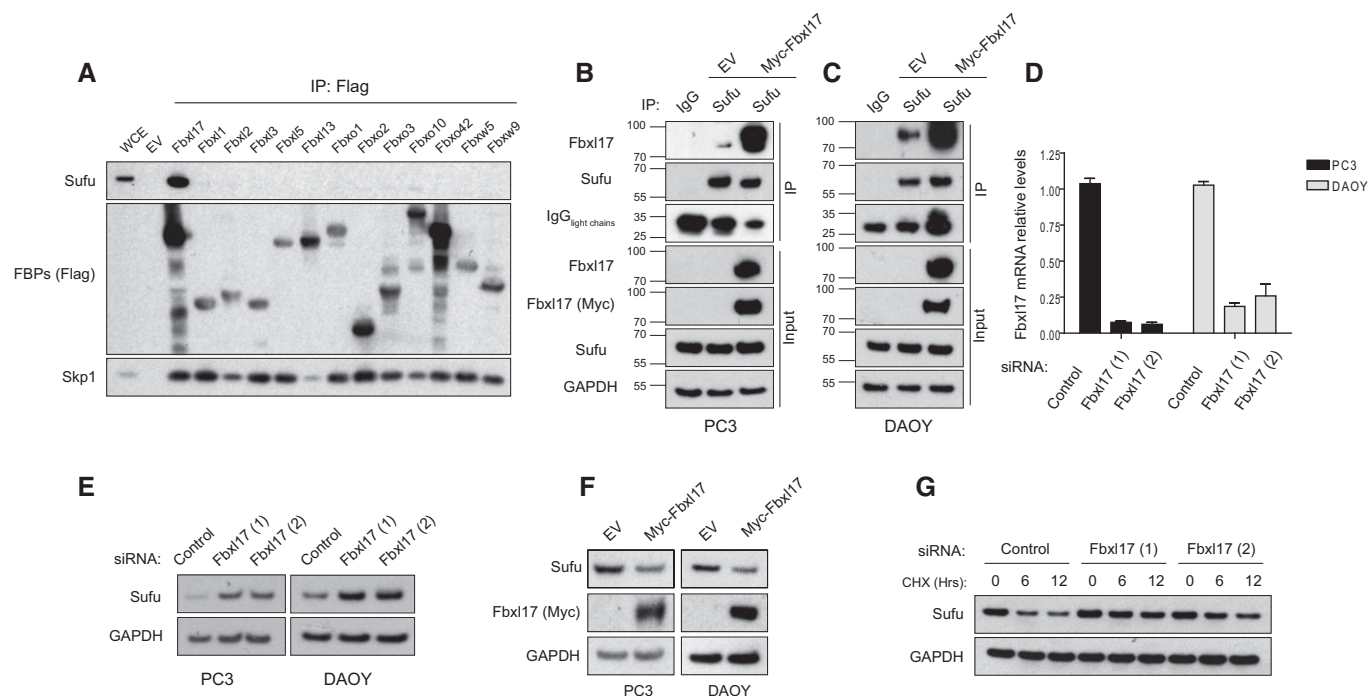


Figure 1. Fbxl17 interacts with Sufu and regulates Sufu levels.

- A** Detection of Sufu and Skp1 after immunoprecipitation of the indicated Flag-tagged F-box proteins (FBPs). An empty vector (EV) was used as a negative control. HEK293T cells were treated with MLN4924 (2 μ M) for 5 h prior to collection. Representative image of three independent experiments is shown.
- B, C** Immunoprecipitation of endogenous Sufu from PC3 (B) and DAOY cells (C) transfected with either an empty vector (EV) or Myc-tagged Fbxl17. Nonspecific rabbit immunoglobulin G (IgG) was used as a negative control. Detection of light chains of immunoglobulin (IgG) was used to assess the amount of IgG used for each immunoprecipitation reaction. Treatment with MLN4925 (2 μ M) was started 5 h before the cell collection.
- D** Quantification of Fbxl17 mRNA levels in PC3 and DAOY cells transfected with a nontargeting siRNA (Control) or two siRNAs to Fbxl17 (1) and (2). The cells were serum-starved for 24 h in serum-reduced medium and treated with SAG (100 nM) for 24 h prior to collection. Data are shown as mean \pm SEM.
- E** Sufu protein levels in PC3 and DAOY cells treated as in (D). GAPDH was used as a loading control. Representative image of three independent experiments is shown.
- F** Sufu protein levels in PC3 and DAOY cells infected with an empty backbone retrovirus (EV) or a retrovirus expressing Myc-tagged Fbxl17. Representative image from three independent experiments is shown.
- G** Detection of Sufu protein levels following cycloheximide (CHX) treatment for the indicated hours, and Fbxl17 depletion using two different siRNAs (Hrs = h). Representative image of two independent experiments is shown.

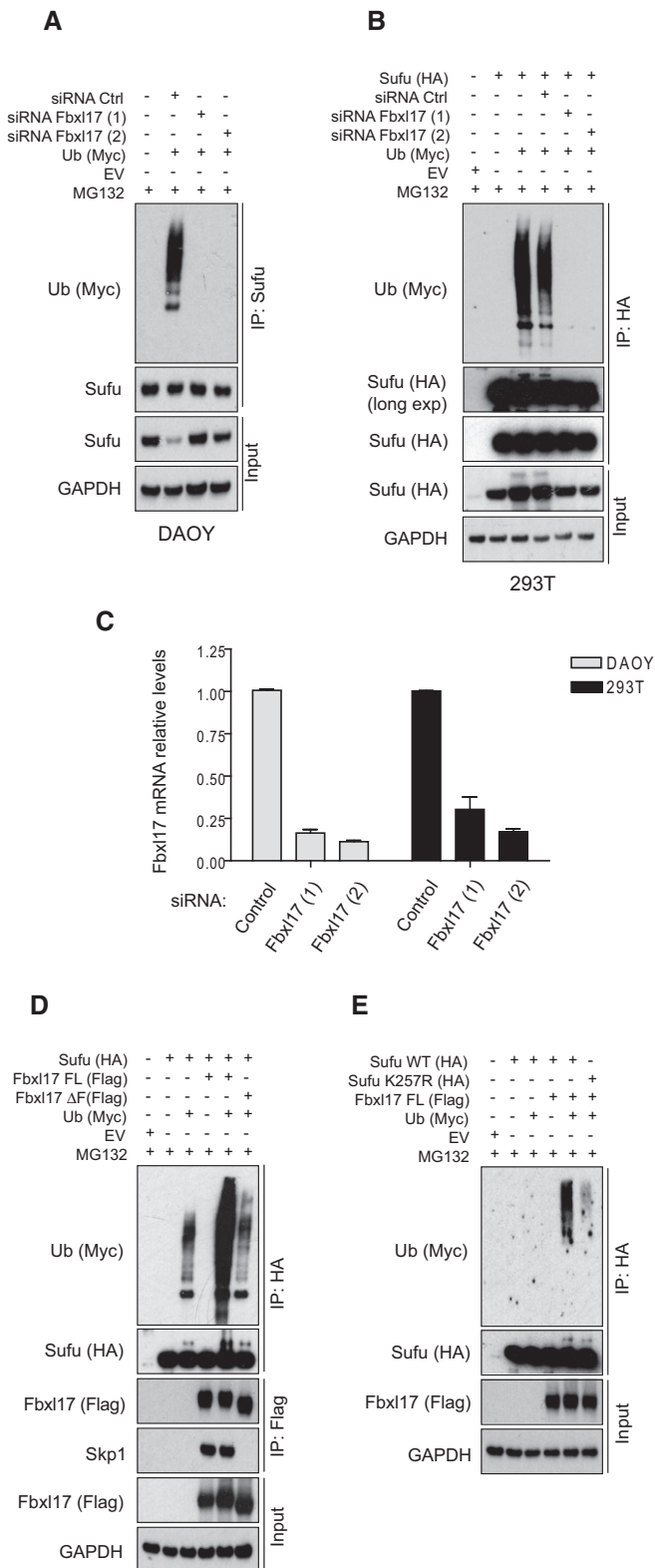
To confirm that the binding between Fbxl17 and Sufu was not due to spurious interaction due to Fbxl17 overexpression, we isolated endogenous Sufu after treating cells with an inhibitor of NAE (Nedd8-activating enzyme) (MLN4924) (Soucy *et al.*, 2009). This treatment blocks cullin neddylation required for the activity of SCF ubiquitin ligases (Ohh *et al.*, 2002). Using this approach, we detected endogenous Fbxl17 in Sufu immunoprecipitates (Fig 1B and C, lane 2) using an antibody against the endogenous protein. To confirm the validity of the antibody for immunoprecipitation and Western blot, we compared Fbxl17 detected in Sufu-immunoprecipitated material to an Fbxl17, which was exogenously expressed (Fig 1B and C, lane 3). The interaction between endogenous Fbxl17 and Sufu was validated in PC3 (human prostate cancer cell line) and DAOY (medulloblastoma cancer cell line) (Fig 1B and C), indicating that Fbxl17 and Sufu interact specifically, physiologically, and in different cell lines.

To assess whether Fbxl17 affects Sufu levels, we measured the protein levels of Sufu in PC3 and DAOY cells upon Fbxl17 depletion using short interfering RNA (siRNA) (Fig 1D). Fbxl17 depletion by two siRNAs increased Sufu protein levels in both PC3 and DAOY (Fig 1E). Opposite to this, exogenous expression of Myc-tagged

Fbxl17 led to the downregulation of Sufu protein in both cell lines (Fig 1F). Sufu protein levels upon either Fbxl17 depletion or overexpression were quantified (Fig EV1A and B). Sufu mRNA levels remained unchanged upon the modulation of Fbxl17 levels (Fig EV1C and D), suggesting that Sufu is regulated by Fbxl17 through a post-translational mechanism. To exclude other mechanisms of control on Sufu by Fbxl17, we measured Sufu half-life in cells where Fbxl17 was depleted using two different siRNAs. While Sufu half-life was approximately 6 h in cells treated with a nontargeting siRNA, this increased to more than 12 h in Fbxl17-depleted cells (Fig 1G). Protein levels of Sufu, upon CHX treatment, were quantified in Fig EV1E and mRNA levels of Fbxl17 were measured by qPCR in Fig EV1F.

SCF^{Fbxl17} mediates Sufu polyubiquitylation

In order to assess whether Fbxl17 is directly targeting Sufu, we measured Sufu polyubiquitylation in cells where Fbxl17 was depleted by siRNA. Remarkably, Sufu polyubiquitylation was completely abolished by Fbxl17 siRNA in both DAOY and 293T cells (Fig 2A–C), supporting the role of Fbxl17 as the major

**Figure 2. SCF^{Fbx17} mediates Sufu polyubiquitylation.**

- A** Detection of polyubiquitylated species of endogenous Sufu co-immunopurified from DAOY cells transfected with Myc-tagged ubiquitin (Ub) either in the presence of nontargeting siRNA (Control) or in the presence of two siRNAs against Fbx17 (1) and (2). MG132 (10 μM) was added in all samples.
- B** Detection of polyubiquitylated species of Sufu upon co-transfection of HEK293T cells with HA-tagged Sufu and Myc-tagged ubiquitin (Ub) either in the presence of nontargeting siRNA (Control) or in the presence of two siRNAs against Fbx17 (1) and (2). MG132 (10 μM) was added in all samples.
- C** Fbx17 mRNA relative levels in DAOY and HEK293T cells upon Fbx17 depletion with either a nontargeting siRNA (Control) or two siRNAs to Fbx17 (1) and (2). Data are shown as mean ± SEM.
- D** Detection of ubiquitylated Sufu co-immunoprecipitated from HEK293T cells co-transfected with HA-tagged Sufu, Myc-ubiquitin (Ub) along with either Flag-tagged Fbx17 wild type (WT) or a mutant lacking the F-box domain (Fbx17ΔF). MG132 (10 μM) was added in all samples.
- E** Detection of ubiquitylated Sufu co-immunoprecipitated from HEK293T cells co-transfected with Myc-tagged ubiquitin (Ub), Flag-tagged Fbx17, and HA-tagged Sufu WT or Sufu mutant K257R. MG132 (10 μM) was added in all samples.

binding, whereas the amino terminus and the F-box motif of Fbx17 were dispensable for Sufu recruitment (Fig EV2A and B). To confirm that polyubiquitylation of Sufu was due to Fbx17 activity, we measured Sufu polyubiquitylation using an Fbx17 lacking the F-box domain (that is still able to interact with Sufu, but not with Skp1; Fig EV2B). Expression of exogenous Fbx17 promoted Sufu polyubiquitylation, whereas an Fbx17 mutant lacking the F-box failed to do so, indicating that the formation of the SCF is not a prerequisite for the binding of Fbx17 to its substrates, but required for ubiquitylation (Fig 2D).

Furthermore, we observed that Fbx17 used the lysine 257 of Sufu as a preferential attachment site for ubiquitin, since the polyubiquitylation of Sufu mutant K257R was impaired (Fig 2E). Using reticulocyte lysates, we reconstituted the components of the SCF^{Fbx17} and Sufu in an *in vitro* reaction, as previously done (Peschiaroli *et al*, 2006). We observed ubiquitylation of Sufu wild type (WT), while the Sufu K257R was ubiquitylated to a reduced extent (Fig EV2C). These findings explain the increased half-life of Sufu K257R mutant reported elsewhere (Yue *et al*, 2009) and suggest that F-box proteins might have preferential ubiquitin attachment sites on substrates.

Fbx17–Sufu interaction is impaired by Sufu phosphorylation and favored by the presence of Gli

To gain insights into the details of Fbx17 recognition of Sufu, we used Sufu-truncated mutants and measured binding to Fbx17. A region of Sufu encompassing amino acids 350–425 was found to be sufficient for the binding to Fbx17 (Fig EV3A–C). Phosphorylation is a common mechanism used by F-box proteins for substrate recognition; however, in the case of Fbxls, phosphorylation could also block substrate recognition (Kuchay *et al*, 2013; Skaar *et al*, 2013).

Sufu WT was unable to bind Fbx17 efficiently as the Sufu 350–484-truncated mutant (Fig EV3B), suggesting the presence of a phosphorylation event on Sufu, that might prevent Fbx17 binding outside of the minimal binding region. Thus, we systematically mutagenized all the serine and threonine residues to alanine on Sufu between the residues 1 and 350. While the majority of sites did

physiological ubiquitin ligase for Sufu in different cellular systems.

Deletion mapping analysis showed that the carboxyl terminus of Fbx17 containing the leucine zipper motif is essential for Sufu

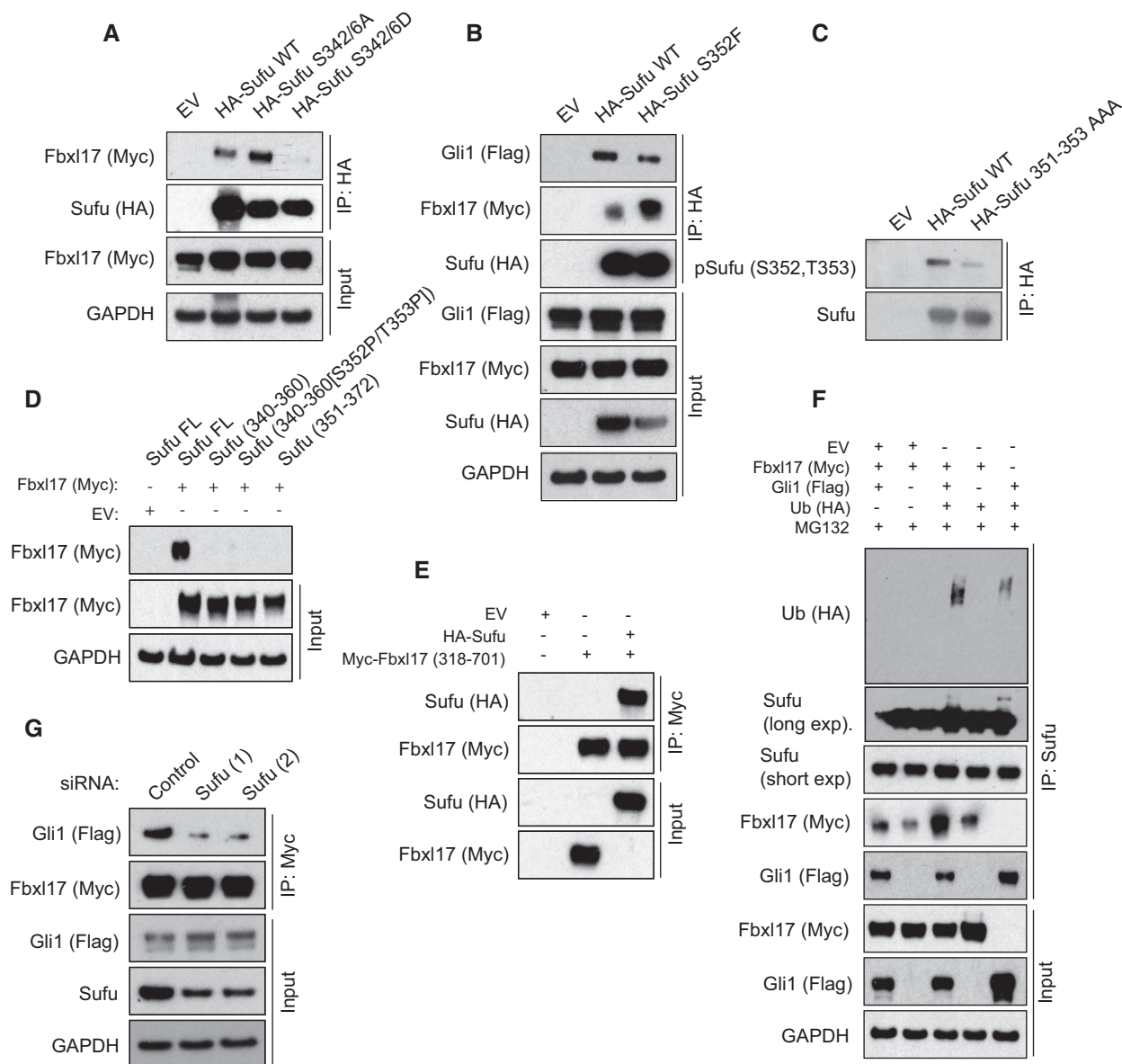


Figure 3. Fbxl17–Sufu interaction is impaired by Sufu phosphorylation and favored by the presence of Gli.

A Detection of Myc-tagged Fbxl17 after immunoprecipitation of HA-tagged Sufu WT or Sufu S342/6A and S342/6D, as indicated. HEK293T cells were treated with MLN4924 (2 μ M) for 5 h prior to collection.

B Detection of Flag-tagged Gli1 and Myc-tagged Fbxl17 binding to immunoprecipitated HA-tagged Sufu wild type (WT) or to Sufu S352F. An empty vector (EV) was used as a negative control. HEK293T cells were treated with MLN4924 (2 μ M) for 5 h prior to collection.

C Detection of Sufu phosphorylated on S352/T353 after immunoprecipitation of HA-tagged Sufu WT and Sufu 351–353 AAA, as indicated.

D Detection of Myc-tagged Fbxl17 binding to Sufu full-length (FL) or to the following Sufu peptides: Sufu 340–360 [APSRKDSLESSTAIIPHEL]; Sufu 340–360 [S352P/T353P] (phosphorylated on the residues S352 and T353); Sufu 351–372 [SSTAIIPHELIRTRQLESVHLK].

E Detection of HA-tagged Sufu binding to a Myc-tagged Fbxl17 construct encompassing the residues 318–701 (corresponding to the F-box motif and C-terminus region) assessed by *in vitro* binding assay. Both proteins were synthesized *in vitro* using a T7-coupled reticulocyte lysate system.

F Detection of ubiquitylated Sufu immunoprecipitated from HEK293T cells co-transfected with HA-tagged ubiquitin (Ub), Myc-tagged Fbxl17, and Flag-tagged Gli1. MG132 (10 μ M) was added in all samples.

G Detection of Flag-tagged Gli1 binding to Myc-tagged Fbxl17 co-immunoprecipitated from HEK293T cells transfected with a non-targeting siRNA (Control) or two siRNA to Sufu (1) and (2), as indicated.

not affect the binding of Fbxl17 to Sufu (Fig EV3E and F), a mutant of Sufu in which the S342 and S346 residues were changed to alanine (A) increased binding to Fbxl17 (Fig 3A). Substitution of S342 and S346 to D (S342/6D) to mimic phosphorylation decreased

recognition by Fbxl17 (Fig 3A). These data are consistent with the increased stabilization of Sufu detected upon the phosphorylation of these residues by PKA (protein kinase A) and GSK3 β (glycogen synthase kinase 3 β) (Chen *et al*, 2011).

Within the minimal binding region of Sufu to Fbx17, Sufu has been found phosphorylated on S352 (Hsu *et al*, 2011). A natural occurring mutation (S352F) abolishing S352 phosphorylation has been described in the medulloblastoma of patients affected by Gorlin syndrome (Smith *et al*, 2014). Therefore, we tested Fbx17 binding to Sufu S352F. The Sufu S352F substitution increased Fbx17 binding (Fig 3B); on the contrary, a mutant of Sufu where the S352 residue was changed to aspartate (D) to mimic the phosphorylation showed reduced binding to Fbx17 (Fig EV3D). We performed LC/MS analysis to obtain high coverage of Sufu modifications and identified multiple phosphorylation sites in this region (Appendix Fig S1A). Furthermore, we generated a phospho-specific antibody against a peptide of Sufu containing both S352 and T353 residues phosphorylated. The antibody recognizes Sufu WT, indicating that S352 and T353 are phosphorylated *in vivo*, but did not recognize a mutant of Sufu where S352 and T353 were substituted to alanine (S351-T353AAA) (Fig 3C).

Given the crucial role of residues S342, S346, and S352 for Fbx17–Sufu interaction, we tested whether Fbx17 is able to bind to a linear peptide encompassing amino acids 340–360 (with and without the phosphorylation of S352/T353 residues) and 351–372. Independently of the phosphorylation status of S352 residue, Fbx17 purified from the cells did not bind to Sufu peptides, but interacted with full-length Sufu *in vitro*, indicating that a linear sequence is not sufficient for Fbx17 binding (Fig 3D). Additionally, Fbx17 and Sufu synthesized *in vitro* were able to bind, pinpointing that the interaction is direct and independent of post-translational modifications induced by Hh signaling (Fig 3E).

Fbxws utilize the WD40 domain to interact with phosphorylated linear degradation sequences; however in the case of the Fbxls, the leucine zipper motif is contacting a larger surface and could require the presence of cofactors (Hao *et al*, 2005; Xing *et al*, 2013). The conformation of Sufu is regulated by Gli binding and Sufu–Gli interaction requires an intact tertiary structure of Sufu (Cherry *et al*, 2013; Zhang *et al*, 2013). Thus, we asked whether Gli1 acts as a cofactor modulating the interaction between Fbx17 and Sufu *in vivo*. Remarkably, Fbx17 polyubiquitylation of endogenous Sufu was favored by the presence of exogenous Gli1 that promoted an increased binding of Fbx17 to Sufu and the subsequent polyubiquitylation (Fig 3F). To assess that the latter was due to the direct interaction between Fbx17 and Sufu, we depleted Sufu using two different siRNA and tested the binding of Gli1 to Fbx17. Sufu

depletion abolished the binding of Gli1 to Fbx17, indicating that Sufu bridges the interaction between Fbx17 and Gli1 *in vivo* (Fig 3G).

Sufu ubiquitylation by Fbx17 allows Gli dissociation for Hedgehog signaling activation

It is not well understood how Sufu is released from Gli1 for full Hh pathway activation. We speculated that Fbx17 could mediate the release by promoting Sufu polyubiquitylation and degradation. To assess the latter, we analyzed Sufu protein levels in mouse embryonic fibroblasts (MEFs) that express the receptor Ptch1 (*Ptch1*^{+/+}), MEFs with heterozygous loss of *Ptch1* (*Ptch1*^{+/-}), and MEFs deficient in *Ptch1* (*Ptch1*^{-/-}), which have constitutive Hh signaling (Taipale *et al*, 2000). Strikingly, MEFs *Ptch1*^{-/-} and *Ptch1*^{+/-} cells showed a decrease in Sufu levels corresponding to the degree of Ptch loss and the consequent Hh activation. Sufu levels were reduced in *Ptch1*^{-/-} and less significantly in *Ptch1*^{+/-}, while remained unaffected in *Ptch1*^{+/+}, indicating that Fbx17 is acting downstream of Ptch and Smo. Low levels of Sufu present in MEFs *Ptch1*^{+/-} and MEFs *Ptch1*^{-/-} were restored to levels comparable to *Ptch1*^{+/+} by Fbx17 depletion (Fig 4A and B). Furthermore, MEFs *Ptch1*^{-/-} lacking Fbx17 presented low transcription levels of Hh target genes such as Gli1 and Bcl2 due to a negative effect that Sufu accumulation exerts on Gli-mediated target gene expression (Fig 4C and D).

Considering the defects observed in pathway activation upon Fbx17 depletion in MEFs *Ptch1*^{-/-} cells and that Fbx17 preferentially binds to the Sufu–Gli complex, we speculated that Fbx17 polyubiquitylation favors Sufu–Gli complex dissociation to allow the need to be substituted with Hh pathway activation. Indeed, Fbx17 overexpression induced Sufu degradation and Gli1 release, whereas the depletion of Fbx17 in MEFs *Ptch1*^{-/-} led to an accumulation of Sufu–Gli1 complexes (Fig 4E and Appendix Fig S1B). Since the polyubiquitylation of Sufu precedes degradation, this model is in accordance with previous findings on Sufu–Gli complex formation and dissociation (Tukachinsky *et al*, 2010).

Finally, we addressed where the degradation of Sufu takes place in cells MEFs *Ptch1*^{-/-} where the pathway is constitutively activated. Due to the lack of an antibody detecting endogenous Fbx17 by immunofluorescence, we stably expressed Fbx17 using a retroviral system that maintains physiological levels of protein expression. To avoid localization artifacts, we expressed an Fbx17 tagged with

Figure 4. Sufu ubiquitylation by Fbx17 allows Gli dissociation for Hedgehog signaling activation.

- Sufu protein levels in mouse embryonic fibroblasts (MEFs) *Ptch1*^{+/+}, *Ptch1*^{+/-}, and *Ptch1*^{-/-} transfected with a nontargeting siRNA (Control) or two siRNAs targeting mouse Fbx17 (1) and (2).
- Quantification of Fbx17 mRNA levels in MEFs *Ptch1*^{+/+}, *Ptch1*^{+/-}, and *Ptch1*^{-/-} transfected as in (A). Data are shown as mean ± SEM.
- Analysis of Gli1 mRNA levels in MEFs *Ptch1*^{+/+} and *Ptch1*^{-/-} upon Fbx17 depletion using two different siRNAs (mean ± SEM from three independent experiments, ****P* < 0.0005, unpaired *t*-test).
- Analysis of Bcl2 mRNA levels in MEFs *Ptch1*^{+/+} and *Ptch1*^{-/-} upon Fbx17 depletion using two different siRNAs (mean ± SEM from three independent experiments, ***P* < 0.005, ****P* < 0.0005, unpaired *t*-test).
- Detection of Flag-tagged Gli1 binding to HA-tagged Sufu in MEFs *Ptch1*^{-/-} upon expression of Myc-tagged Fbx17, or Fbx17 depletion by two siRNAs. For each condition, 200 μg of whole-cell lysate was immunoprecipitated.
- Immunostaining of Fbx17 using anti-Myc antibody in *Ptch1*^{-/-} MEFs stably transduced with a pBABE vector expressing Fbx17 tagged with Myc either at the N-terminus [Myc(N)-Fbx17] or at the C-terminus [Myc(C)-Fbx17]. Scale bars: 20 μm.
- Detection of Fbx17 using anti-Myc antibody in *Ptch1*^{-/-} MEFs stably expressing Myc(N)-Fbx17 (Fbx17 tagged at the N-terminus) and Myc(C)-Fbx17 (Fbx17 tagged at the C-terminus).
- Detection of HA-tagged Fbx17 binding to endogenous Sufu immunoprecipitated from cytoplasmic and nuclear extracts from *Ptch1*^{-/-} MEFs. Asterisk (*) indicates a nonspecific band. Identification of cytoplasmic and nuclear fractions was performed by lamin A/C and GAPDH detection.

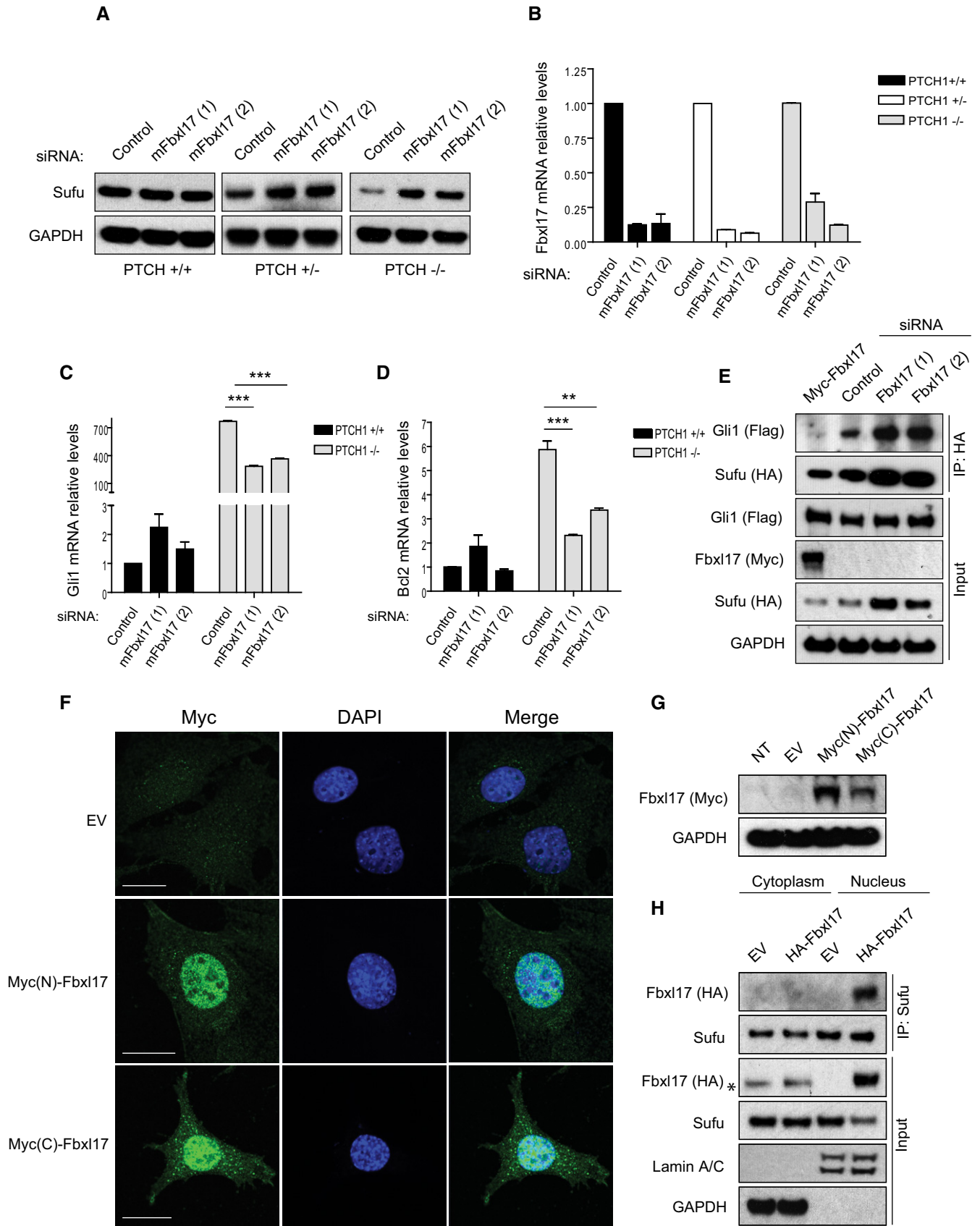


Figure 4.

Myc at the C-terminus and N-terminus. In both cases, the localization of Fbxl17 in MEFs *Ptch1*^{-/-} was exclusively nuclear (Fig 4F and G). Furthermore, exogenous Fbxl17 expressed in MEFs *Ptch1*^{-/-} induced downregulation of Sufu in the nucleus, where Fbxl17 interacted with Sufu upon biochemical fractionation of the cytoplasmic and nuclear extracts (Fig 4H). Since phosphorylation of Sufu on S342/S346 promotes ciliary retention of Sufu (Chen *et al*, 2011), these data are in accordance with a model where Sufu dephosphorylation promotes the localization outside the cilium and ubiquitin mediated proteolysis by Fbxl17.

Fbxl17-mediated degradation of Sufu regulates Hh signaling, cancer cell proliferation, and medulloblastoma growth

Given the relevant role of Fbxl17 in regulating Hh signaling and that Hh signaling activity has been implicated in the proliferation of prostate cancer cell lines (Karhadkar *et al*, 2004; Sanchez *et al*, 2004), we further tested the effect of Fbxl17 on Hh activation by quantifying Gli1 mRNA levels upon either depletion or expression of Fbxl17 using PC3 cells. Fbxl17 silencing resulted in a decrease in Gli1 mRNA levels (Appendix Fig S2A), and contrarily, Fbxl17 expression led to an increase in Gli1 mRNA levels (Appendix Fig S2B). Since proliferation of PC3 cells is in part dependent on Hh signaling pathway (Karhadkar *et al*, 2004; Zhang *et al*, 2007), we evaluated whether Fbxl17 depletion impairs the prostate cancer cell proliferation. Fbxl17 silencing induced a defective cell proliferation of PC3 cells and this defect was rescued by the reintroduction of Fbxl17 full length in cells depleted of Fbxl17 (Appendix Fig S2C–F). Moreover, this phenotype was dependent on the accumulation of Sufu, as double siRNA of Fbxl17 and Sufu could restore the proliferation (Appendix Fig S3A–D).

A more direct role of Hh pathway has been established in the pathogenesis of medulloblastoma characterized by the presence of mutations in central components of Hh signaling (Kool *et al*, 2014); therefore, we tested whether the Fbxl17–Sufu axis operates in medulloblastoma cancer cells. DAOY human medulloblastoma cells have been reported to be responsive to Hh signaling modulation (Gotschel *et al*, 2013). DAOY cells responded to Smo activation (using SAG; Smo agonist) or inhibition (using cyclopamine; Smo antagonist) by upregulating or downregulating Gli1 mRNA levels, respectively (Fig EV4A). Silencing of Fbxl17 impaired Gli1 transcription upon SAG-induced Hh activation (Fig EV4B–D). Additionally, upon the stimulation of DAOY cells with SHH (Sonic Hedgehog)-conditioned media (Fig EV4E), Sufu protein levels were reduced (Fig EV4F). Fbxl17 depletion restored Sufu protein levels after SHH-conditioned media (Fig EV4F and quantified in EV4G), confirming that the downstream activation of Hh signaling pathway depends on Fbxl17-mediated degradation of Sufu in DAOY cells. The observed downregulation of Sufu protein was not due to the variation in Fbxl17 expression upon Hh stimulation. Indeed, the mRNA of Fbxl17 was not affected in DAOY cells upon Hh stimulation with SAG or SHH ligand and Hh inhibition with cyclopamine (Fig EV4H and I).

Similar to PC3 cells, we evaluated whether Fbxl17 depletion impairs DAOY cell proliferation. Proliferation of DAOY cells was hampered by Fbxl17 depletion and stimulated by Fbxl17 re-expression (Fig 5A). Fbxl17 siRNA (quantified in Fig 5B) increased protein levels of Sufu; on the contrary, expression of Fbxl17 corresponded to low protein levels of Sufu in DAOY (Fig 5C and Appendix Fig

S4A). Importantly, the proliferation defect induced by Fbxl17 depletion was dependent on the accumulation of Sufu, as double siRNA of Fbxl17 and Sufu could restore proliferation in DAOY (Fig 5D–F and Appendix Fig S4B).

To investigate the relevance of Fbxl17–Sufu axis in cancer, we assessed the effect of RNAi of Fbxl17 *in vivo* by using an orthotopic rat model of medulloblastoma. Fbxl17 RNAi led to an impaired Hh signaling reflected by the accumulation of Sufu protein and decreased Gli1 mRNA (Fig 6A–C and Appendix Fig S5A).

In vivo T₂-weighted magnetic resonance imaging (MRI) showed a marked reduction in tumor progression over time with RNAi against Fbxl17 (Fig 6D and E). In contrast, the area of gadolinium enhancement on T₁-weighted images at the end-point showed no differences between groups (Appendix Fig S5B and C). Histologically, tumors with RNAi against Fbxl17 showed significantly reduced growth compared to a nontargeting control as detected by vimentin staining (6.1 ± 1.7 mm² vs. 12.4 ± 1.3 mm²; *P* < 0.05; Fig 6F and G), and also a significantly lower proliferative index within the tumor tissue (5.4 ± 3.6% vs. 20.8 ± 2.8%; *P* < 0.05; Fig 5H and I). Together, these data suggest that T₂-weighted MRI may be more sensitive to inhibition of tumor growth than post-contrast T₁-weighted MRI in this setting.

Fbxl17–Sufu axis is altered in medulloblastoma

According to the gene transcription profiles, four different subtypes of medulloblastoma have been described, that is, wingless type (Wnt), Sonic Hedgehog (SHH), group 3, and group 4 (Gajjar & Robinson, 2014). The SHH subtype of medulloblastoma is characterized by an increased Hh signaling due to the altered expression of pathway components. Given the relevant role of Fbxl17 in Hh signaling and medulloblastoma growth, we analyzed the mRNA expression of Fbxl17 and Sufu reported in the largest published medulloblastoma expression profiling study (*N* = 285 primary samples) (Northcott *et al*, 2012). Although Sufu has a pivotal role in Hh signaling and mutations in Sufu are present in SHH medulloblastoma, the mRNA of Sufu was found to be not reduced in the SHH subtype, whereas Gli1 was found to be drastically increased (Fig 7A and B). Strikingly, Fbxl17 mRNA was found to be significantly increased in the SHH-subtype medulloblastoma (Fig 7C) and the levels of Fbxl17 and Gli1 positively correlated (Spearman's rho = 0.5640; *P* < 0.00001; Fig 7D). In the absence of Sufu mRNA alterations, these results suggest that in medulloblastoma the control of Sufu protein levels by Fbxl17 plays a prominent role in sustaining Hh activation.

The distinction of four molecular subgroups depends on the transcriptional profiles of the subgroups, which at least for SHH subtype reflects the cells of origin of the medulloblastoma. In the SHH subtype is established that granule cell progenitors (GCPs) represent the cell of origin of the malignancy (Wechsler-Reya & Scott, 1999; Marino *et al*, 2000; Oliver *et al*, 2005; Schuller *et al*, 2008). Thus, we tested the effect of siRNA and the expression of Fbxl17 in GCPs. Similar to the results obtained in DAOY, Fbxl17 expression increased cell proliferation (Fig EV5A and B); on the contrary, siRNA of Fbxl17 reduced cell proliferation measured by BrdU incorporation (Fig EV5C and D).

To establish a role for Fbxl17 in the etiology of medulloblastoma through Sufu mutation, we investigated in more detail the Sufu

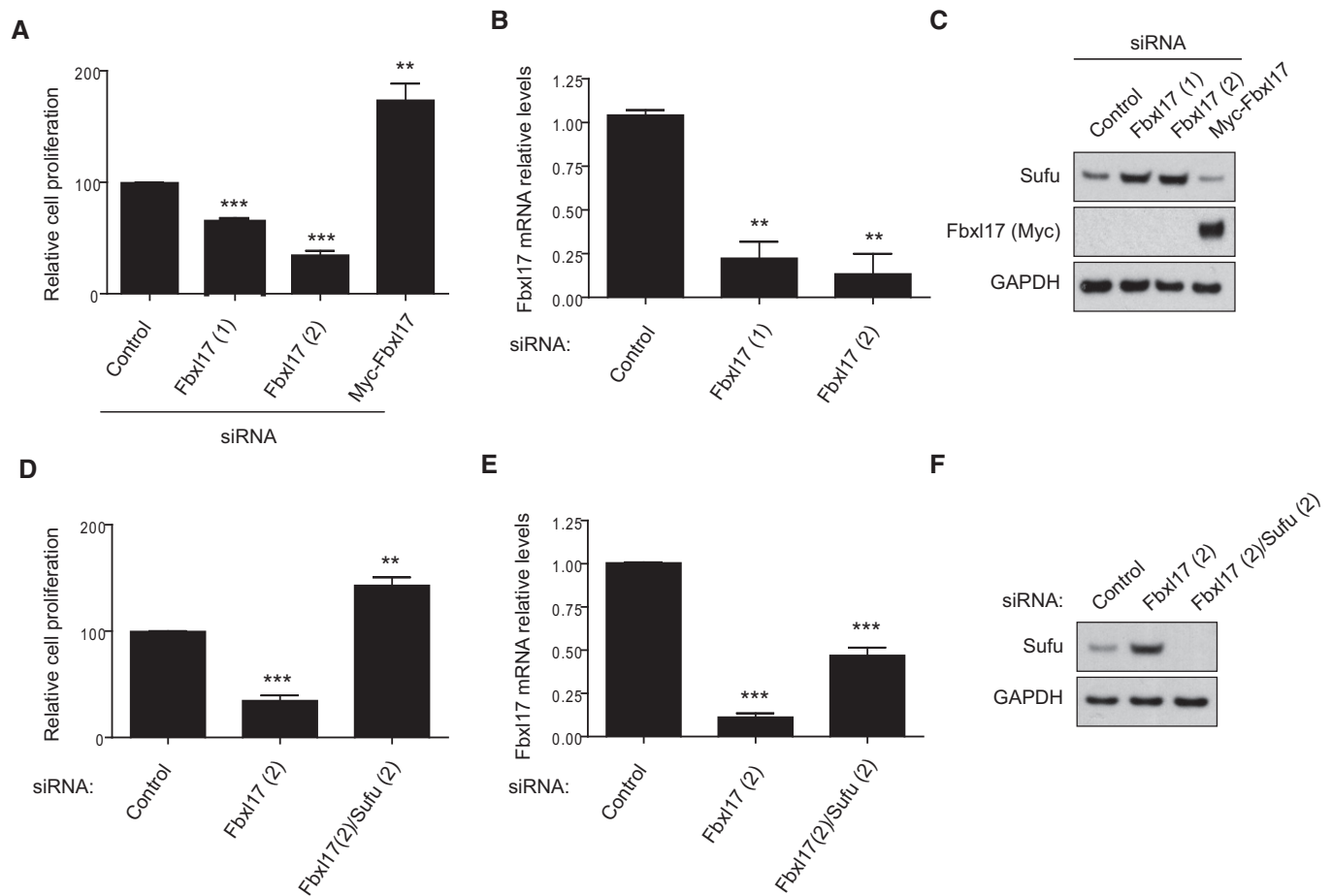


Figure 5. Fbx17-mediated degradation of Sufu promotes medulloblastoma cell proliferation.

- A Cell proliferation of DAOY cells upon Fbx17 depletion using a nontargeting siRNA (Control), two siRNAs against Fbx17 (1) and (2) or upon reintroduction of a Myc-tagged Fbx17 construct in Fbx17-depleted DAOY cells using siRNA Fbx17 (2) (mean \pm SEM from three independent experiments, ** P < 0.005; *** P < 0.0005, unpaired t -test).
- B Quantification of Fbx17 mRNA levels in DAOY cells transfected with a nontargeting siRNA (Control) or two siRNAs against Fbx17 (1) and (2) (mean \pm SEM from three independent experiments, ** P < 0.005, unpaired t -test).
- C Sufu protein levels in DAOY cells treated as in (A). Representative image of three independent experiments is shown.
- D Cell proliferation of DAOY cells transfected with nontargeting siRNA (Control), siRNA against Fbx17 or a combination of siRNA targeting Fbx17 and Sufu (mean \pm SEM from three independent experiments, ** P < 0.005; *** P < 0.0005, unpaired t -test).
- E Quantification of Fbx17 mRNA levels in DAOY cells treated as in (D) (mean \pm SEM from three independent experiments, *** P < 0.0005, unpaired t -test).
- F Sufu protein levels in DAOY cells treated as in (D). Representative image of three independent experiments is shown.

Source data are available online for this figure.

S352F substitution, which favors binding to Fbx17 (Fig 3A). This substitution appears in the medulloblastoma of patients affected by Gorlin syndrome and contributes to the medulloblastoma development, in the absence of other alterations in Hh pathway (Smith *et al*, 2014). We observed that the half-life of Sufu S352F was found to be decreased compared to Sufu WT, in accordance with an increased binding to Fbx17. Furthermore, silencing of Fbx17 restored Sufu mutant half-life (Fig 7E). Using firefly luciferase-based Gli-reporter assay (Sasaki *et al*, 1997), we assessed the effect of Sufu S352F on Hh activation in MEFs *Sufu*^{-/-} reconstituted with either Sufu WT or SufuS352F. Strikingly, Sufu S352F increased the responsiveness of cells to Hh agonist (SAG) (Fig 7F), indicating that the faster proteolysis of Sufu, mediated by Fbx17, has a functional role in the control of Hh signaling.

These observations exemplify the role of Fbx17–Sufu axis alterations in medulloblastoma.

Discussion

Our findings identify Fbx17 as a novel regulator of Hh signaling pathway. Fbx17 mediates Sufu polyubiquitylation and degradation through the proteasome. The interaction between Fbx17 and Sufu is hampered by the phosphorylation of Sufu on S342 and S346 residues, which were shown to be target sites for PKA and GSK3 β , respectively (Chen *et al*, 2011) (Fig 8A). Phosphorylation of Sufu retains it in the primary cilium (Chen *et al*, 2011) and could represent a failsafe mechanism to avoid unscheduled pathway activation

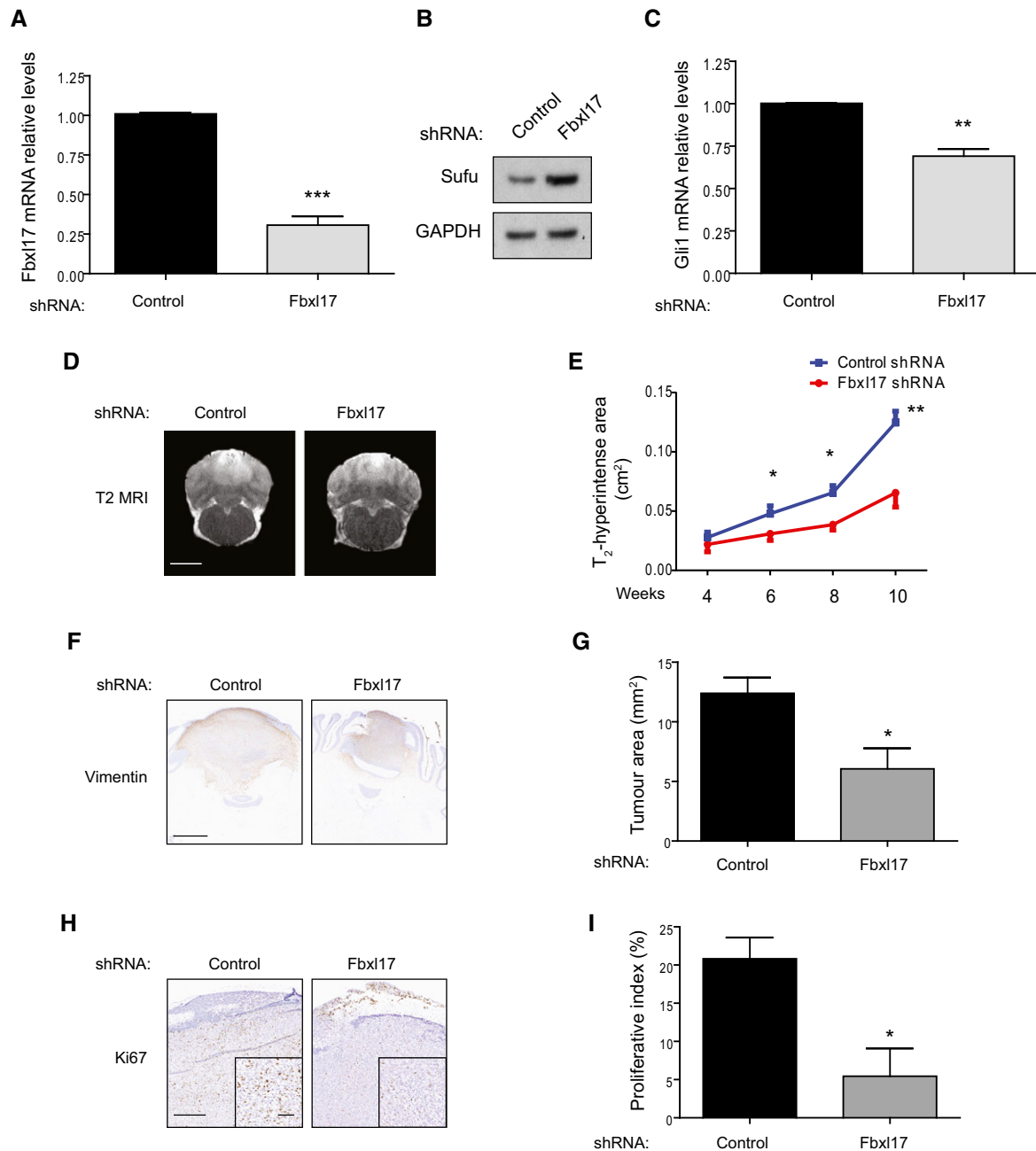


Figure 6. Fbx17-mediated degradation of Sufu promotes medulloblastoma tumor growth.

- A Quantification of Fbx17 mRNA levels in DAOY cells transfected with control shRNA or shRNA targeting Fbx17 (mean \pm SEM from three independent experiments, *** P < 0.0005, unpaired t -test).
- B Detection of Sufu protein levels in DAOY cells transfected with control shRNA or shRNA Fbx17. Representative image of three independent experiments is shown.
- C Quantification of Gli1 mRNA levels in DAOY cells transfected with control shRNA or shRNA Fbx17 (mean \pm SEM from three independent experiments, ** P < 0.005, unpaired t -test).
- D T_2 -weighted magnetic resonance images showing tumor development in rats injected with DAOY cells transfected with control shRNA or shRNA against Fbx17. One representative image for each condition at 10 weeks is shown. Scale bar: 5 mm.
- E Graph showing area of T_2 hyperintensity (a surrogate marker of tumor growth) between 4 and 10 weeks post-tumor induction. Animals were injected with DAOY cells stably expressing control shRNA or shRNA against Fbx17 (10,000 cells/ μ l) (mean \pm SEM; n = 5; two-way ANOVA, followed by unpaired t -test, * P < 0.05, ** P < 0.01).
- F Representative immunohistochemical image of vimentin staining. Scale bar: 1 mm.
- G Quantification of tumor growth (vimentin staining) in rats injected with DAOY cells transfected with either control shRNA or shRNA against Fbx17 (mean \pm SEM; n = 5; unpaired t -test, * P < 0.05).
- H Representative immunohistochemical image of Ki67 staining. Scale bar: 0.5 mm/0.1 mm.
- I Quantification of proliferative index (Ki67 staining) in rats injected with DAOY cells transfected with either control shRNA or shRNA against Fbx17 (mean \pm SEM; n = 5; unpaired t -test, * P < 0.05).

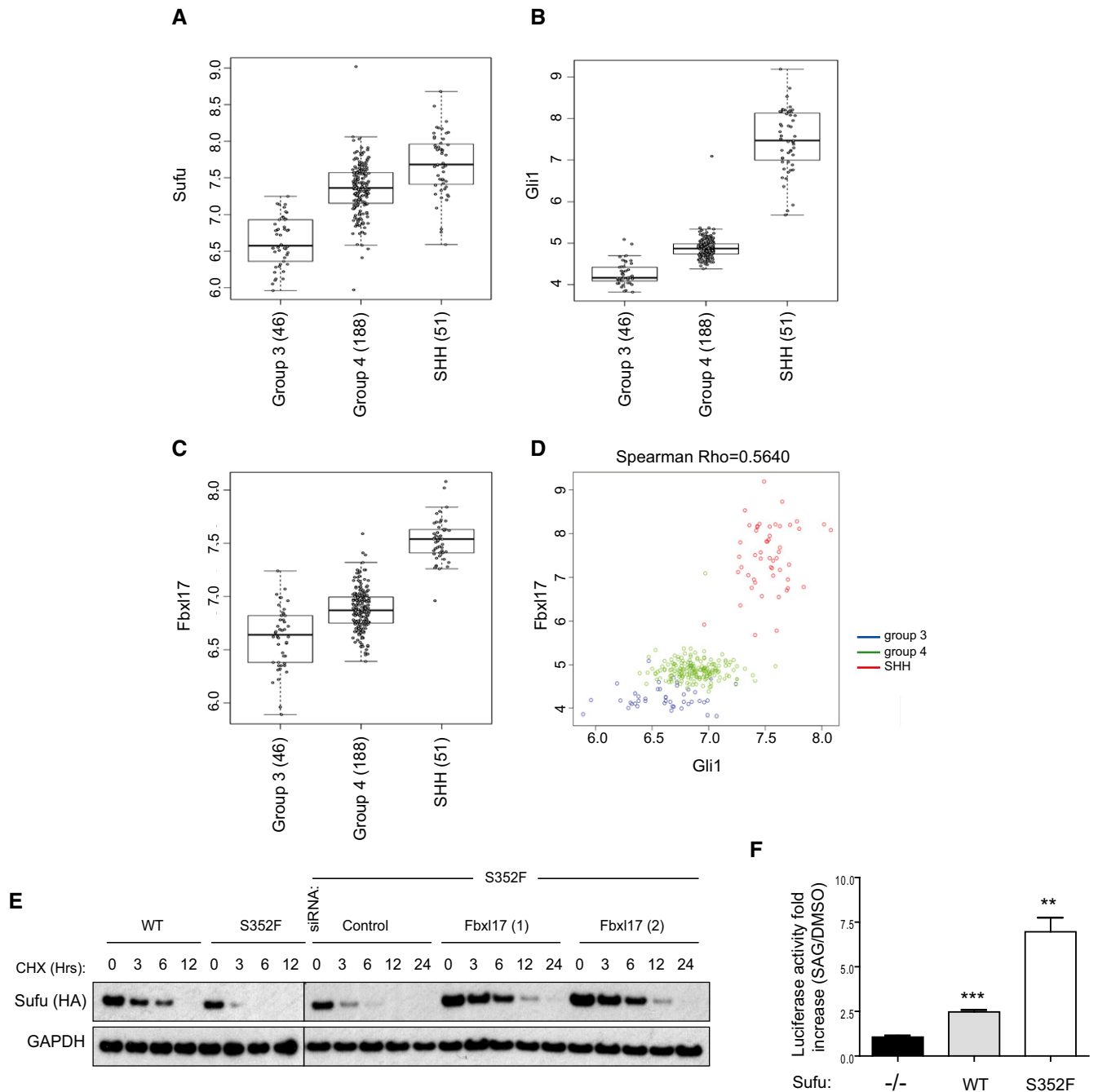


Figure 7. Fbxl17–Sufu axis is altered in medulloblastoma.

A–C mRNA expression of Sufu, Gli1, and Fbxl17 detected in 285 medulloblastoma samples (GEO accession: GSE37382), stratified by tumor subtype. Level of significance (P) for Kruskal–Wallis (KW) rank test is $P < 10^{-8}$. Analysis using one-way ANOVA gave comparable results (median \pm 1.5 interquartile distance).

D Expression of Gli1 and Fbxl17 in the 285 patients is shown colored by subgroup; level of significance (P) for Kruskal–Wallis (KW) rank test is $P < 10^{-8}$, and Spearman's rank correlation ($R = 0.5640$) is indicated.

E Detection of HA-tagged Sufu wild type (WT) and HA-tagged Sufu S352F protein levels in NIH3T3 cells after cycloheximide (CHX) treatment. Where indicated, the cells were transfected with a nontargeting siRNA (Control) or two siRNA to Fbxl17 (1) and (2). Representative image of three independent experiments is shown.

F Assessment of Hh pathway activation using Gli1–luciferase reporter assay in MEFs *Sufu*^{-/-} upon the reintroduction of HA-tagged Sufu WT or Sufu mutant S352F using a retroviral system (mean \pm SEM from three independent experiments, ** $P < 0.005$; *** $P < 0.0005$, unpaired t -test).

when the Hh ligands are not present. A similar but opposite mechanism of regulation is operated downstream of Sufu at the levels of Gli2 and Gli3 by the SCF β Trcp ubiquitin ligase. In this case, the

concerted action of PKA and GSK3 β generates a phosphorylation-dependent signal for ubiquitylation by β Trcp (Bhatia *et al*, 2006; Wang & Li, 2006). The ubiquitylation of Gli2 and Gli3 generates

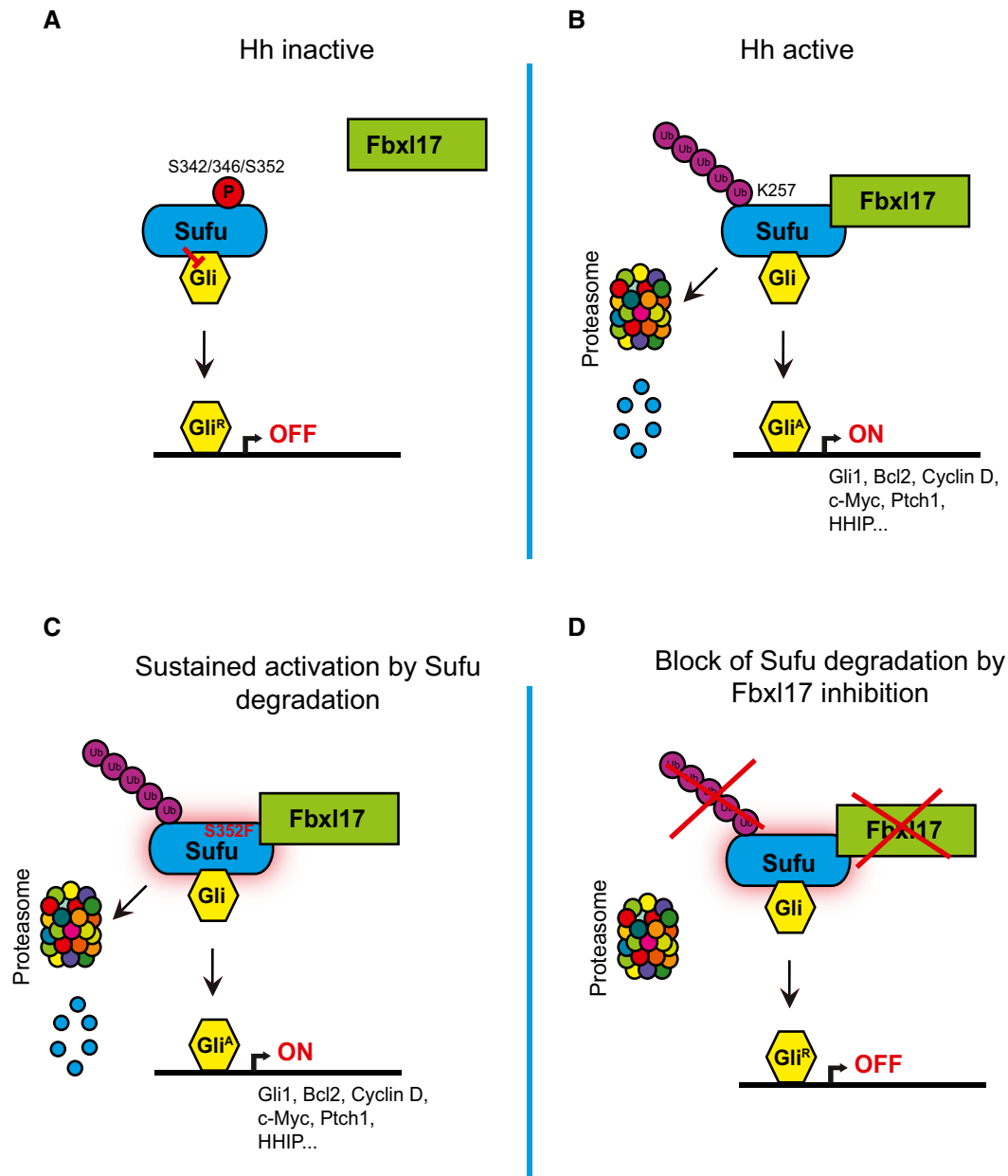


Figure 8. SCF (Fbx17) ubiquitylation of Sufu regulates Hedgehog signaling and medulloblastoma growth.

A–D Scheme outlining the mechanism of Sufu recognition by Fbx17 and its alteration in medulloblastoma.

transcriptional repressors to avoid pathway activation. Thus, PKA and GSK3 β act on multiple components of Hh pathway as general negative regulators (Chen & Jiang, 2013).

Upon Hh ligand binding to Ptch1, a swift activation of the pathway entails the reversal of PKA and GSK3 β phosphorylation on Sufu S342 and S346, in addition to S352/T353. The dephosphorylation of Sufu initiates Fbx17 polyubiquitylation of Sufu on lysine 257 for proper signal transduction (Fig 8B). Sufu is upstream of Gli processing (Humke *et al*, 2010), and thus, it is tantalizing to speculate that the dephosphorylation of Sufu promotes Gli dephosphorylation for the formation of transcriptional activators. In

medulloblastoma, increased expression of Fbx17 and substitution in critical Sufu residues (S352F), required for Fbx17 binding, allow amplified pathway activation and increased cell proliferation (Fig 8C). Inhibition of Fbx17 blocks Sufu degradation, Hh pathway activation and prevents medulloblastoma tumor growth (Fig 8D).

An important feature of Fbx17–Sufu axis is that Fbx17 acts preferentially on Sufu in complex with Gli1, thus selecting for degradation an active pool of Sufu. Upon Hh signaling activation, Fbx17-mediated polyubiquitylation of Sufu induces Sufu–Gli complex dissociation for the transduction of the Hh signal.

Sufu protein levels are exquisitely sensitive to the degree of Hh activation, indicating that the regulation of Sufu levels by Fbx17 adds a further layer of control for the generation of more refined transcriptional programs in physiological conditions. Indeed, Fbx17 could regulate Sufu levels to fine-tune transcriptional outputs; however, more studies are required to establish how the upstream components of the pathway regulate Sufu and Fbx17. At the same time, it is noteworthy that Fbx17 transcription is blocked by methylation in embryonic stem cells and transcribed in neural stem cells where Hh plays a more active role (Cortese *et al*, 2011). In line with this, Fbx17 expression is increased in the brain and spinal cord during development (Diez-Roux *et al*, 2011), pointing out to a role for Fbx17 in physiological development. Furthermore, a putative homolog of Fbx17 (CG31633) has been described in *D. melanogaster*, where the absence of the latter induces a pupal lethal phenotype (Dui *et al*, 2012), suggesting an essential role of Fbx17 in development.

Mutations in the components of Hh signaling are a feature of SHH medulloblastoma (Kool *et al*, 2014). We show that in a case of familial medulloblastoma, altered proteolysis of Sufu plays an active role in the induction of sustained Hh signaling. Importantly, mutations in other components of Hh signaling pathway, such as Ptch (present in > 50% of SHH medulloblastoma) (Kool *et al*, 2014), will also affect Sufu protein levels, given the effect of pathway activation on Sufu protein mediated by Fbx17. Thus, in the majority of SHH medulloblastoma, Sufu protein levels will be low due to the constitutive activation of Hh signaling. In these cancers, increasing Sufu levels through Fbx17 inhibition could block Hh signaling and cell proliferation. Overexpression of Fbx17 in SHH subgroups provides a therapeutic window to selectively target cancer cells. Thus, our study highlights Fbx17 as a novel target for the treatment of SHH medulloblastoma.

Other mutations of Sufu residing in critical residues for Fbx17 binding have been described in colorectal cancer and malignant melanoma (Krauthammer *et al*, 2012; Giannakis *et al*, 2014); thus, alteration in Fbx17–Sufu axis could be present in other cancer types. The biological significance of these alterations for cell proliferation remains to be determined in these cancers. The use of Smo inhibitors for the treatment of medulloblastoma is being tested in the clinic with encouraging results (Robinson *et al*, 2015), but could be significantly prevented by the acquisition of resistance through secondary Smo mutations, described in basal cell carcinoma and medulloblastoma (Yauch *et al*, 2009; Atwood *et al*, 2015; Sharpe *et al*, 2015). In medulloblastoma, the combination of Smo inhibitors and Fbx17 inhibitors could be a viable alternative strategy to obtain sustained responses.

Our findings pave the way for the investigation of therapies targeting the ubiquitin proteasome system in the treatment for medulloblastoma and other cancers relying on Hh signaling.

Materials and Methods

Cell culture

All cell lines were routinely cultured in a humidified incubator at 37°C under 5% CO₂ in the indicated culture medium containing 10% fetal bovine serum (FBS, Sigma Aldrich) supplemented with

100 U/ml penicillin sodium and 100 µg/ml streptomycin sulfate (Sigma Aldrich).

HEK293T, HeLa (ATCC, American Type Culture Collection), and DAOY cells (kind gift from Dr. Maike Glitsch, Department of Physiology, Anatomy and Genetics, University of Oxford, UK) were grown in Dulbecco's modified Eagle's medium (DMEM, Gibco/Invitrogen), while PC3 cells (kindly provided by Dr. Richard Bryant from Ludwig Institute for Cancer Research, University of Oxford, UK) were maintained in RPMI 1640 (Lonza). *Ptch1*^{+/+}, *Ptch1*^{+/-}, and *Ptch1*^{-/-} mouse embryonic fibroblasts (MEFs, kind gift from Dr. Philip Beachy, Department of Biochemistry, Stanford University), *Sufu*^{-/-} MEFs (kindly provided by Dr. Stephan Teglund, Department of Biosciences and Nutrition, Karolinska Institutet, Sweden), and NIH3T3 cells (ATCC) were cultured in DMEM supplemented with 1 mM sodium pyruvate (Sigma Aldrich) and 0.1 mM MEM nonessential amino acids (Sigma Aldrich).

Hh pathway assays and production of SHH-conditioned medium

Hyperconfluent DAOY, PC3 cells, and *Sufu*^{-/-} MEFs were starved for 24 h in serum-reduced medium (DMEM with 0.5% FBS), and subsequently, the Hh signaling pathway was stimulated using Smoothed agonist SAG (100 nM, Calbiochem) or Sonic Hedgehog (SHH)-conditioned medium (1:4). For Hh signaling inhibition, cyclopamine (Sigma Aldrich) was added to the starvation medium at a final concentration of 10 µM. DMSO (dimethyl sulfoxide) was used as a solvent and as control vehicle. *Ptch1*^{+/+}, *Ptch1*^{+/-}, and *Ptch1*^{-/-} MEFs were assessed after 24 h of maintenance in serum-starved in serum-reduced medium. SHH-conditioned medium was generated as described previously (Cherry *et al*, 2013). After 24 h of incubation with the appropriate Hh pathway agonists, antagonist, or control vehicle, cell cultures were harvested for real-time PCR or Western blotting.

Antibodies

The following monoclonal antibodies were used: anti-Myc (9B11, mouse, Cell Signaling Technology), anti-HA (05-904, mouse, Millipore and 16B12, Biolegend), anti-Sufu (C81H7, rabbit, Cell Signaling Technology), anti-lamin A/C (4C11, Cell Signaling Technology), and anti-vimentin (V9, mouse, Vector Laboratories). Polyclonal antibodies were used as follows: anti-Flag (F7425, rabbit, Sigma Aldrich), anti-Fbx17 (PA5-31396, rabbit, Thermo Fisher Scientific Pierce), anti-GAPDH (MA5-15738, rabbit, Sigma Aldrich), anti-Sufu (C-15, goat, Santa Cruz Biotechnology), anti-Ki67 (SP6, rabbit, Vector Laboratories), and anti-Skp1 (kind gift from Dr. Michele Pagano at NYU Cancer Institute, New York University School of Medicine, USA). A rabbit polyclonal antibody against the following peptide of Sufu was raised Hu #347~360: CLESDS-pS-pT-AIIPHEL. To ensure the specific recognition of phosphorylated Sufu, the antibody was affinity-purified against a phosphorylated peptide and absorbed against a nonphosphorylated peptide CLESDSSTAIPHEL.

Liquid chromatography–tandem mass spectrometry (LC-MS/MS) analysis

Flag/Myc-tagged Fbx17 co-immunopurified material was eluted by competition using Flag peptide. Supernatant material was subjected

to two rounds of chloroform–methanol precipitation as described (Wessel & Flugge, 1984). Samples were then resuspended in 6 M urea, 100 mM ammonium acetate pH ~8 and subjected to in-solution trypsin digestion and analysis by nano-liquid chromatography–tandem mass spectrometry as described previously (Ternette *et al*, 2013). In brief, after solubilization of the sample pellets, 3 µl of trypsin (20 ng/µl, Promega) was added to the samples diluted six times with H₂O for an overnight digestion at 37°C. The samples were then desalted using a C18 SEP PAK cartridge according to the manufacturer's instructions (Waters), dried via Speed Vac centrifugation, and resuspended in 20 µl of a 2% CH₃CN/0.1% TFA solution. Peptides were analyzed by nano-liquid chromatography–tandem mass spectrometry (nano-LC-MS/MS) using a Nano-Acquity-UPLC (C18 column with a 75 µm × 250 mm, 1.7 µm particle size; Waters) coupled to an Orbitrap Velos tandem mass spectrometer (Thermo Scientific, Bremen, Germany) with a resolution of 70,000 full-width half maximum at mass/charge 400, top 15 precursor ion selection, and fragmentation performed in collision-induced dissociation (CID) mode. The samples were loaded in 99.5% buffer A (0.1% FA in H₂O). The gradient used to elute the peptides started by a 3-min isocratic gradient composed of 3% buffer B (0.1% FA in CH₃CN) followed by a linear gradient from 3–40% of buffer B for 60 min at a flow rate of 250 nl/min and a two washes with 97% of buffer B for 3 min. The total length of the analysis was 100 min to allow the column re-equilibration. The raw MS data were converted into Mascot generic files using MSconvert (Kessner *et al*, 2008). Searches were performed using Matrix Science software using the following parameters: The error tolerance was fixed at 20 ppm for precursor ions and at 0.5 Da for fragment ions. The enzyme used was trypsin and only one missed cleavage was allowed. MS data were searched against the human uniprot-swissprot database (UniProt_SwissProt, human 20,353 sequences) in which the false discovery rate (FDR) was estimated using a decoy database approach (Mascot) and set to 1%.

***In vivo* and *in vitro* ubiquitylation assay**

HEK293T cells were plated in 10-cm culture dishes at 80% confluence, and 24 h later, the cells were transfected with the indicated plasmids and incubated for 48 h. The cells were treated with MG132 (10 µM) for 5 h prior to collection. For Fbx17 silencing, two rounds of siRNA transfections were performed, and the plasmids were delivered to the cells along with the siRNA duplexes in the first round of transfection. Twenty-four hours after the second round of transfection, the cells were treated with MG132 and collected 5 h later. The cells were lysed in LB and ubiquitylated Sufu was co-immunoprecipitated using either anti-HA or anti-Sufu antibody coupled to Protein G agarose beads. Polyubiquitinated forms of Sufu were detected by immunoblot using anti-Myc or anti-HA as indicated.

In vitro ubiquitylation assay was performed using proteins translated in a reticulocyte system, as previously done for SCF βTrcp (Dorrello *et al*, 2006). Myc-tagged Fbx17 (318–701) and Sufu WT or Sufu K257R were *in vitro* translated using TnT Quick Coupled Transcription/Translation System reticulocyte system from Promega according to the manufacturer's instructions. After translation, Fbx17 was mixed with Sufu WT or Sufu K257R in a volume of 40 µl containing 0.1 µM E1 (Boston Biochem), 10 ng/µl Ubch3,

10 ng/µl Ubch5c, 1 µM ubiquitin aldehyde, 2.5 µg/µl ubiquitin (Sigma), in a ubiquitylation buffer (50 mM Tris pH 7.6, 2 mM ATP, 5 mM MgCl₂, 0.6 mM DTT, okadaic acid 0.1 µM). The reaction mixtures were incubated at 30°C for the indicated times and analyzed by Western blot of Sufu as indicated.

***In vitro* binding assay**

HA-tagged Sufu full-length and Myc-tagged-Fbx17 construct 318–701 was *in vitro*-transcribed and translated using TNT[®] Quick Coupled Transcription/Translation System (Promega) according to the manufacturer's instructions. Proteins were incubated on ice for 1 h followed by co-immunoprecipitation of Myc-tagged Fbx17, using anti-Myc antibody, in binding buffer containing 50 mM Tris–HCl pH 7.5, 100 mM NaCl, 2 mM EDTA, 0.1% NP-40, and protease inhibitors. Reactions were stopped with Laemmli buffer and resolved by SDS–PAGE.

Sufu peptides Sufu (340–360), Sufu (340–360) phosphorylated on S352 and T353, and Sufu (351–372) (synthesized by ChinaPeptides Co., Ltd.) were conjugated to CNBr-activated Sepharose (GE Healthcare) according to the supplier's specifications. HA-tagged Sufu full length synthesized as described above and bound to Protein G–Sepharose beads was used as a positive control. Cell lysates of HEK293T cells transfected with Myc-tagged Fbx17 were used to assess the binding to Sufu peptides using standard co-immunoprecipitation procedures.

***In vivo* medulloblastoma model**

DAOY cells transfected with either scrambled shRNA or shRNA against Fbx17 were cultured until approximately 80–90% confluent and then resuspended in PBS for intracerebral injection.

Two cohorts ($n = 5$ per group) of male nude rats (Harlan, France), 3–4 weeks old, were injected intracerebrally in the cerebellar vermis (–11 mm posterior and 0 mm lateral to Bregma, and depth 1 mm) using a finely drawn glass microcapillary (< 100 µm tip). Animals were anaesthetized with 2–3% isoflurane in a mixture of nitrous oxide and oxygen (50%/50%) and placed in a stereotaxic frame (Stoelting Co.). A midline incision was made in the scalp and a burr hole drilled. The animals were injected with 10⁴ cells in 1 µl over a 10-min period. At the end of the injection, the needle was left in place for 2 min before being slowly removed. Following injection, the scalp wound was closed and the animals were allowed to recover from anesthesia.

Magnetic resonance imaging

MRI was performed using a horizontal bore 9.4T magnet with a Varian DirectDrive™ (Agilent Technologies, Santa Clara, CA, USA). The animals were anesthetized with 1–2% isoflurane in 70% N₂/30% O₂ and a cannula positioned in the tail vein for gadolinium-DTPA (Gd-DTPA) injection. The animals were positioned in a quadrature volume transmit coil (i.d. 72 mm) with four phased-array surface receiver coils (i.d.: 40 mm, RAPID Biomedical GmbH) and placed in the magnet. Body temperature and respiration were monitored throughout and maintained at ~37°C and 50 breaths per min, respectively. Multiparametric MRI was acquired including the acquisition of T₁-weighted images pre- and post-Gd-DTPA injection

to assess the blood–brain barrier (BBB) integrity, and T₂-weighted images to determine the macroscopic changes in tissue structure, as previously described (Serres *et al*, 2014). Briefly, T₂-weighted images were acquired using a fast spin-echo sequence with a repetition time (TR) of 3.0 s and an effective echo time (TE) of 60 ms. Spin-echo T₁-weighted images (TR = 500 ms; TE = 20 ms) were acquired both before and 5 min after the injection of 100 µl Gd-DTPA (Omniscan®, GE Healthcare, UK). The matrix size and field of view were 256 × 256 and 3.5 × 3.5 cm, respectively. In all cases, a multi-slice acquisition was used, spanning the cerebellum with axial slice thickness of 1 mm.

Regions of interest (ROI) encompassing areas of visible signal change in the cerebellar vermis were drawn on both the T₂-weighted and post-Gd-DTPA T₁-weighted images, and the areas were calculated.

Statistical analysis

Quantitative analysis of band intensity was performed using the Image J program. Data are reported as mean ± SEM. Statistical analyses were performed using GraphPad Prism (GraphPad Software, Inc.). Differences between the groups were compared using unpaired Student's *t*-test.

Affymetrix Human Gene 1.1 ST Array profiling of 285 primary medulloblastoma samples (Northcott *et al*, 2012) was obtained from Gene Expression Omnibus database (<http://www.ncbi.nlm.nih.gov/geo>), accession: GSE37382. Normalized, logged base 2, gene expression determined using Affymetrix Expression Console (1.1) as previously described (Northcott *et al*, 2012) was considered. One-way ANOVA and Kruskal–Wallis tests were both used to test the equality of expression values between the groups. Spearman's rank correlation test was used to test the gene expression association. Data analysis was performed using R.

Expanded View for this article is available online.

Acknowledgements

This study was possible thanks to the support of Medical Research Council (MRC) Grant MC_PC_12007 to V.D'A; Cancer Research UK Grant C5255/A12678 to N.R.S.; and grant support to R.T. from the Swedish Research Council, the Swedish Cancer Society, and the Center for Innovative Medicine at Karolinska Institutet. This work was supported by a John Fell (133/075) and Wellcome Trust Grant (097813/Z/11/Z) to B.M.K. and AIRC Grant IG#14723 to L.D.M. We thank Dr. Christian Siebold for the *Sufu* cDNA and advice.

Author contributions

MR performed most of the biochemical experiments and analyses of cell growth, and EF helped with the biochemical studies. SS, CB, and NRS designed, performed, and analyzed the animal studies. LDM and PI performed the GCPs study. BMK, RF, and M-LT performed the LC/MS analysis of Fbxl17-interacting proteins. RT and CF provided reagents, protocols, and expert advice for Hh stimulation/experiments. FMB and AB analyzed Fbxl17–Sufu–Gli1 levels in medulloblastoma. JCC provided expert advice on *in vitro* ubiquitylation experiments. VDA and MR wrote the manuscript. VDA coordinated the study and oversaw all experiments. All authors discussed the results, commented on and assisted in revising the manuscript.

Conflict of interest

The authors declare that they have no conflict of interest.

References

- Atwood SX, Sarin KY, Whitson RJ, Li JR, Kim G, Rezaee M, Ally MS, Kim J, Yao C, Chang AL, Oro AE, Tang JY (2015) Smoothed variants explain the majority of drug resistance in basal cell carcinoma. *Cancer Cell* 27: 342–353
- Bassermann F, Eichner R, Pagano M (2014) The ubiquitin proteasome system – implications for cell cycle control and the targeted treatment of cancer. *Biochim Biophys Acta* 1843: 150–162
- Bhatia N, Thiyagarajan S, Elcheva I, Saleem M, Dlugosz A, Mukhtar H, Spiegelman VS (2006) Gli2 is targeted for ubiquitination and degradation by beta-TrCP ubiquitin ligase. *J Biol Chem* 281: 19320–19326
- Chen Y, Yue S, Xie L, Pu XH, Jin T, Cheng SY (2011) Dual Phosphorylation of suppressor of fused (*Sufu*) by PKA and GSK3beta regulates its stability and localization in the primary cilium. *J Biol Chem* 286: 13502–13511
- Chen Y, Jiang J (2013) Decoding the phosphorylation code in Hedgehog signal transduction. *Cell Res* 23: 186–200
- Cherry AL, Finta C, Karlstrom M, Jin Q, Schwend T, Astorga-Wells J, Zubarev RA, Del Campo M, Criswell AR, de Sanctis D, Jovine L, Toftgard R (2013) Structural basis of SUFU–GLI interaction in human Hedgehog signalling regulation. *Acta Crystallogr D Biol Crystallogr* 69: 2563–2579
- Cooper AF, Yu KP, Brueckner M, Brailey LL, Johnson L, McGrath JM, Bale AE (2005) Cardiac and CNS defects in a mouse with targeted disruption of suppressor of fused. *Development* 132: 4407–4417
- Cortese R, Lewin J, Backdahl L, Krispin M, Wasserkort R, Eckhardt F, Beck S (2011) Genome-wide screen for differential DNA methylation associated with neural cell differentiation in mouse. *PLoS ONE* 6: e26002
- D'Angiolella V, Donato V, Forrester FM, Jeong YT, Pellacani C, Kudo Y, Saraf A, Florens L, Washburn MP, Pagano M (2012) Cyclin F-mediated degradation of ribonucleotide reductase M2 controls genome integrity and DNA repair. *Cell* 149: 1023–1034
- Diez-Roux G, Banfi S, Sultan M, Geffers L, Anand S, Rozado D, Magen A, Canidio E, Pagani M, Peluso I, Lin-Marq N, Koch M, Bilio M, Cantiello I, Verde R, De Masi C, Bianchi SA, Cicchini J, Perroud E, Mehmeti S *et al* (2011) A high-resolution anatomical atlas of the transcriptome in the mouse embryo. *PLoS Biol* 9: e1000582
- Dorrello NV, Peschiaroli A, Guardavaccaro D, Colburn NH, Sherman NE, Pagano M (2006) S6K1- and betaTRCP-mediated degradation of PDCD4 promotes protein translation and cell growth. *Science* 314: 467–471
- Dui W, Lu W, Ma J, Jiao R (2012) A systematic phenotypic screen of F-box genes through a tissue-specific RNAi-based approach in *Drosophila*. *J Genet Genomics* 39: 397–413
- Dunaeva M, Michelson P, Kogerman P, Toftgard R (2003) Characterization of the physical interaction of Gli proteins with SUFU proteins. *J Biol Chem* 278: 5116–5122
- Gajjar AJ, Robinson GW (2014) Medulloblastoma-translating discoveries from the bench to the bedside. *Nat Rev Clin Oncol* 11: 714–722
- Giannakis M, Hodis E, Jasmine Mu X, Yamauchi M, Rosenbluh J, Cibulskis K, Saksena G, Lawrence MS, Qian ZR, Nishihara R, Van Allen EM, Hahn WC, Gabriel SB, Lander ES, Getz G, Ogino S, Fuchs CS, Garraway LA (2014) RNF43 is frequently mutated in colorectal and endometrial cancers. *Nat Genet* 46: 1264–1266
- Gotschel F, Berg D, Gruber W, Bender C, Eberl M, Friedel M, Sonntag J, Rungeler E, Hache H, Wierling C, Nietfeld W, Lehrach H, Frischauf A,

- Schwartz-Albiez R, Aberger F, Korf U (2013) Synergism between Hedgehog-Gli and EGFR signaling in Hedgehog-responsive human medulloblastoma cells induces downregulation of canonical Hedgehog-target genes and stabilized expression of GLI1. *PLoS ONE* 8: e65403
- Guardavaccaro D, Kudo Y, Boulaire J, Barchi M, Busino L, Donzelli M, Margottin-Goguet F, Jackson PK, Yamasaki L, Pagano M (2003) Control of meiotic and mitotic progression by the F box protein beta-Trcp1 *in vivo*. *Dev Cell* 4: 799–812
- Hao B, Zheng N, Schulman BA, Wu G, Miller JJ, Pagano M, Pavletich NP (2005) Structural basis of the Cks1-dependent recognition of p27(Kip1) by the SCF(Skp2) ubiquitin ligase. *Mol Cell* 20: 9–19
- Hooper JE, Scott MP (2005) Communicating with Hedgehogs. *Nat Rev Mol Cell Biol* 6: 306–317
- Hsu PP, Kang SA, Rameseder J, Zhang Y, Ottina KA, Lim D, Peterson TR, Choi Y, Gray NS, Yaffe MB, Marto JA, Sabatini DM (2011) The mTOR-regulated phosphoproteome reveals a mechanism of mTORC1-mediated inhibition of growth factor signaling. *Science* 332: 1317–1322
- Hui CC, Angers S (2011) Gli proteins in development and disease. *Annu Rev Cell Dev Biol* 27: 513–537
- Humke EW, Dorn KV, Milenkovic L, Scott MP, Rohatgi R (2010) The output of Hedgehog signaling is controlled by the dynamic association between Suppressor of Fused and the Gli proteins. *Genes Dev* 24: 670–682
- Ingham PW, Nakano Y, Seger C (2011) Mechanisms and functions of Hedgehog signalling across the metazoa. *Nat Rev Genet* 12: 393–406
- Jin J, Cardozo T, Lovering RC, Elledge SJ, Pagano M, Harper JW (2004) Systematic analysis and nomenclature of mammalian F-box proteins. *Genes Dev* 18: 2573–2580
- Karhadkar SS, Bova GS, Abdallah N, Dhara S, Gardner D, Maitra A, Isaacs JT, Berman DM, Beachy PA (2004) Hedgehog signalling in prostate regeneration, neoplasia and metastasis. *Nature* 431: 707–712
- Kessner D, Chambers M, Burke R, Agus D, Mallick P (2008) ProteoWizard: open source software for rapid proteomics tools development. *Bioinformatics* 24: 2534–2536
- Kijima C, Miyashita T, Suzuki M, Oka H, Fujii K (2012) Two cases of nevoid basal cell carcinoma syndrome associated with meningioma caused by a PTCH1 or SUFU germline mutation. *Fam Cancer* 11: 565–570
- Kogerman P, Grimm T, Kogerman L, Krause D, Unden AB, Sandstedt B, Toftgard R, Zaphiropoulos PG (1999) Mammalian suppressor-of-fused modulates nuclear-cytoplasmic shuttling of Gli-1. *Nat Cell Biol* 1: 312–319
- Kool M, Jones DT, Jager N, Northcott PA, Pugh TJ, Hovestadt V, Piro RM, Esparza LA, Markant SL, Remke M, Milde T, Bourdeaut F, Ryzhova M, Sturm D, Pfaff E, Stark S, Hutter S, Seker-Cin H, Johann P, Bender S et al (2014) Genome sequencing of SHH medulloblastoma predicts genotype-related response to smoothed inhibition. *Cancer Cell* 25: 393–405
- Krauthammer M, Kong Y, Ha BH, Evans P, Bacchicocchi A, McCusker JP, Cheng E, Davis MJ, Goh G, Choi M, Ariyan S, Narayan D, Dutton-Regester K, Capatana A, Holman EC, Bosenberg M, Szoln M, Kluger HM, Brash DE, Stern DF et al (2012) Exome sequencing identifies recurrent somatic RAC1 mutations in melanoma. *Nat Genet* 44: 1006–1014
- Kuchay S, Duan S, Schenkein E, Peschiaroli A, Saraf A, Florens L, Washburn MP, Pagano M (2013) FBXL2- and PTPL1-mediated degradation of p110-free p85beta regulatory subunit controls the PI(3)K signalling cascade. *Nat Cell Biol* 15: 472–480
- Lee Y, Kawagoe R, Sasai K, Li Y, Russell HR, Curran T, McKinnon PJ (2007) Loss of suppressor-of-fused function promotes tumorigenesis. *Oncogene* 26: 6442–6447
- Marino S, Vooijs M, van Der Gulden H, Jonkers J, Berns A (2000) Induction of medulloblastomas in p53-null mutant mice by somatic inactivation of Rb in the external granular layer cells of the cerebellum. *Genes Dev* 14: 994–1004
- Merchant M, Vajdos FF, Ultsch M, Maun HR, Wendt U, Cannon J, Desmarais W, Lazarus RA, de Vos AM, de Sauvage FJ (2004) Suppressor of fused regulates Gli activity through a dual binding mechanism. *Mol Cell Biol* 24: 8627–8641
- Northcott PA, Shih DJ, Peacock J, Garzia L, Morrissy AS, Zichner T, Stutz AM, Korshunov A, Reimand J, Schumacher SE, Beroukhim R, Ellison DW, Marshall CR, Lionel AC, Mack S, Dubuc A, Yao Y, Ramaswamy V, Luu B, Rolider A et al (2012) Subgroup-specific structural variation across 1,000 medulloblastoma genomes. *Nature* 488: 49–56
- Ohh M, Kim WY, Moslehi JJ, Chen Y, Chau V, Read MA, Kaelin WG Jr (2002) An intact NEDD8 pathway is required for Cullin-dependent ubiquitylation in mammalian cells. *EMBO Rep* 3: 177–182
- Oliver TG, Read TA, Kessler JD, Mehmeti A, Wells JF, Huynh TT, Lin SM, Wechsler-Reya RJ (2005) Loss of patched and disruption of granule cell development in a pre-neoplastic stage of medulloblastoma. *Development* 132: 2425–2439
- Pastorino L, Ghiorzo P, Nasti S, Battistuzzi L, Cusano R, Marzocchi C, Garre ML, Clementi M, Scarra GB (2009) Identification of a SUFU germline mutation in a family with Gorlin syndrome. *Am J Med Genet A* 149A: 1539–1543
- Peschiaroli A, Dorrello NV, Guardavaccaro D, Venere M, Halazonetis T, Sherman NE, Pagano M (2006) SCFbetaTrCP-mediated degradation of Claspin regulates recovery from the DNA replication checkpoint response. *Mol Cell* 23: 319–329
- Robinson GW, Orr BA, Wu G, Gururangan S, Lin T, Qaddoumi I, Packer RJ, Goldman S, Prados MD, Desjardins A, Chintagumpala M, Takebe N, Kaste SC, Rusch M, Allen SJ, Onar-Thomas A, Stewart CF, Fouladi M, Boyett JM, Gilbertson RJ et al (2015) Vismodegib exerts targeted efficacy against recurrent sonic hedgehog-subgroup medulloblastoma: results from phase II pediatric brain tumor consortium studies PBTC-025B and PBTC-032. *J Clin Oncol* 33: 2646–2654
- Sanchez P, Hernandez AM, Stecca B, Kahler AJ, DeGueme AM, Barrett A, Beyna M, Datta MW, Datta S, Ruiz i Altaba A (2004) Inhibition of prostate cancer proliferation by interference with SONIC HEDGEHOG-GLI1 signaling. *Proc Natl Acad Sci USA* 101: 12561–12566
- Sasaki H, Hui C, Nakafuku M, Kondoh H (1997) A binding site for Gli proteins is essential for HNF-3beta floor plate enhancer activity in transgenics and can respond to Shh *in vitro*. *Development* 124: 1313–1322
- Schuller U, Heine VM, Mao J, Kho AT, Dillon AK, Han YG, Huillard E, Sun T, Ligon AH, Qian Y, Ma Q, Alvarez-Buylla A, McMahon AP, Rowitch DH, Ligon KL (2008) Acquisition of granule neuron precursor identity is a critical determinant of progenitor cell competence to form Shh-induced medulloblastoma. *Cancer Cell* 14: 123–134
- Serres S, Martin CJ, Sarmiento Soto M, Bristow C, O'Brien ER, Connell JJ, Khrapitchev AA, Sibson NR (2014) Structural and functional effects of metastases in rat brain determined by multimodal MRI. *Int J Cancer* 134: 885–896
- Sharpe HJ, Pau G, Dijkgraaf GJ, Basset-Seguín N, Modrusan Z, Januario T, Tsui V, Durham AB, Dlugosz AA, Haverty PM, Bourgon R, Tang JY, Sarin KY, Dirix L, Fisher DC, Rudin CM, Sofen H, Migden MR, Yauch RL, de Sauvage FJ (2015) Genomic analysis of smoothed inhibitor resistance in basal cell carcinoma. *Cancer Cell* 27: 327–341

- Sheng T, Li C, Zhang X, Chi S, He N, Chen K, McCormick F, Gatalica Z, Xie J (2004) Activation of the hedgehog pathway in advanced prostate cancer. *Mol Cancer* 3: 29
- Skaar JR, D'Angiolella V, Pagan JK, Pagano M (2009) SnapShot: F Box Proteins II. *Cell* 137: 1358, 1358.e1351
- Skaar JR, Pagan JK, Pagano M (2013) Mechanisms and function of substrate recruitment by F-box proteins. *Nat Rev Mol Cell Biol* 14: 369–381
- Skaar JR, Pagan JK, Pagano M (2014) SCF ubiquitin ligase-targeted therapies. *Nat Rev Drug Discovery* 13: 889–903
- Smith MJ, Beetz C, Williams SG, Bhaskar SS, O'Sullivan J, Anderson B, Daly SB, Urquhart JE, Bholah Z, Oudit D, Cheesman E, Kelsey A, McCabe MG, Newman WG, Evans DG (2014) Germline mutations in SUFU cause Gorlin syndrome-associated childhood medulloblastoma and redefine the risk associated with PTCH1 mutations. *J Clin Oncol* 32: 4155–4161
- Soucy TA, Smith PG, Milhollen MA, Berger AJ, Gavin JM, Adhikari S, Brownell JE, Burke KE, Cardin DP, Critchley S, Cullis CA, Doucette A, Garnsey JJ, Gaulin JL, Gershman RE, Lublinsky AR, McDonald A, Mizutani H, Narayanan U, Olhava EJ et al (2009) An inhibitor of NEDD8-activating enzyme as a new approach to treat cancer. *Nature* 458: 732–736
- Svard J, Heby-Henricson K, Persson-Lek M, Rozell B, Lauth M, Bergstrom A, Ericson J, Toftgard R, Teglund S (2006) Genetic elimination of Suppressor of fused reveals an essential repressor function in the mammalian Hedgehog signaling pathway. *Dev Cell* 10: 187–197
- Taipale J, Chen JK, Cooper MK, Wang B, Mann RK, Milenkovic L, Scott MP, Beachy PA (2000) Effects of oncogenic mutations in Smoothed and Patched can be reversed by cyclopamine. *Nature* 406: 1005–1009
- Tan MK, Lim HJ, Bennett EJ, Shi Y, Harper JW (2013) Parallel SCF adaptor capture proteomics reveals a role for SCFFBXL17 in NRF2 activation via BACH1 repressor turnover. *Mol Cell* 52: 9–24
- Taylor MD, Liu L, Raffel C, Hui CC, Mainprize TG, Zhang X, Agatep R, Chiappa S, Gao L, Lowrance A, Hao A, Goldstein AM, Stavrou T, Scherer SW, Dura WT, Wainwright B, Squire JA, Rutka JT, Hogg D (2002) Mutations in SUFU predispose to medulloblastoma. *Nat Genet* 31: 306–310
- Teglund S, Toftgard R (2010) Hedgehog beyond medulloblastoma and basal cell carcinoma. *Biochim Biophys Acta* 1805: 181–208
- Ternette N, Yang M, Laroyia M, Kitagawa M, O'Flaherty L, Wolhuter K, Igarashi K, Saito K, Kato K, Fischer R, Berquand A, Kessler BM, Lappin T, Frizzell N, Soga T, Adam J, Pollard PJ (2013) Inhibition of mitochondrial aconitase by succination in fumarate hydratase deficiency. *Cell Rep* 3: 689–700
- Tukachinsky H, Lopez LV, Salic A (2010) A mechanism for vertebrate Hedgehog signaling: recruitment to cilia and dissociation of SuFu-Gli protein complexes. *J Cell Biol* 191: 415–428
- Wang B, Li Y (2006) Evidence for the direct involvement of β TrCP in Gli3 protein processing. *Proc Natl Acad Sci USA* 103: 33–38
- Wechsler-Reya RJ, Scott MP (1999) Control of neuronal precursor proliferation in the cerebellum by Sonic Hedgehog. *Neuron* 22: 103–114
- Wessel D, Flugge UI (1984) A method for the quantitative recovery of protein in dilute solution in the presence of detergents and lipids. *Anal Biochem* 138: 141–143
- Xing W, Busino L, Hinds TR, Marionni ST, Saifee NH, Bush MF, Pagano M, Zheng N (2013) SCF(FBXL3) ubiquitin ligase targets cryptochromes at their cofactor pocket. *Nature* 496: 64–68
- Yauch RL, Dijkgraaf GJ, Alickie B, Januario T, Ahn CP, Holcomb T, Pujara K, Stinson J, Callahan CA, Tang T, Bazan JF, Kan Z, Seshagiri S, Hann CL, Gould SE, Low JA, Rudin CM, de Sauvage FJ (2009) Smoothed mutation confers resistance to a Hedgehog pathway inhibitor in medulloblastoma. *Science* 326: 572–574
- Yue S, Chen Y, Cheng SY (2009) Hedgehog signaling promotes the degradation of tumor suppressor Sufu through the ubiquitin-proteasome pathway. *Oncogene* 28: 492–499
- Zhang J, Lipinski R, Shaw A, Gipp J, Bushman W (2007) Lack of demonstrable autocrine hedgehog signaling in human prostate cancer cell lines. *J Urol* 177: 1179–1185
- Zhang Y, Fu L, Qi X, Zhang Z, Xia Y, Jia J, Jiang J, Zhao Y, Wu G (2013) Structural insight into the mutual recognition and regulation between Suppressor of Fused and Gli/Ci. *Nat Commun* 4: 2608



License: This is an open access article under the terms of the Creative Commons Attribution 4.0 License, which permits use, distribution and reproduction in any medium, provided the original work is properly cited.

SCF (Fbx17) ubiquitylation of Sufu regulates Hedgehog signaling and medulloblastoma development

APPENDIX - Table of Contents

Additional Materials and Methods

Figure Legends: Appendix Figures S1 – S5

Additional References

Appendix Figures S1-S5

Appendix

Additional Materials and Methods

DNA constructs generation

A cDNA coding full-length *Fbxl17* was purchased from origene (RC228545). For generation of Fbxl17 deletion constructs the appropriate nucleotide fragments carrying a Myc tag at the N-terminus were amplified by polymerase chain reaction (PCR) and cloned into the pcDNA 3.1 (+) plasmid. Additionally, full-length Fbxl17 was 3x FLAG tagged at the N-terminus and cloned into the pcDNA 3.1 (+) vector. This construct was used as template to generate the Fbxl17 Δ F construct as follows: 5'-phosphorylated primers containing an XhoI restriction site at each 5'end were designed to flank the F-box domain of Fbxl17. The PCR product was DpnI digested to eliminate the paternal template and circularized using the T4 DNA ligase (New England Biolabs). Mutant plasmids were transformed into competent *E. coli* (DH5 α gold cells, Bioline). N-terminus Myc-tagged Fbxl17 was cloned into the pQCXIP retroviral expression vector that was used to generate DAOY and PC3 cells stably expressing Fbxl17. Fbxl17 with a Myc tag either at the N-terminus or at the C-terminus, as well as HA-tagged Fbxl17 was cloned into the pBABE Puro retroviral expression vector and used to stably transduced *Ptch*^{-/-} MEFs.

Full-length of human *Sufu* coding sequence (isoform 1, NM_016169.3, generously provided by Dr. Christian Siebold, Nuffield Department of Medicine, University of Oxford, UK) was HA-tagged at the N-terminus and cloned into the pcDNA3.1 (+) vector. N-terminus and C-terminus truncated constructs of Sufu were generated using the above mentioned tag and plasmid. HA-tagged Sufu mutant K257R, as well as all the serine and threonine mutants used in this study, were generated from the full-length construct using the QuikChange site-directed

mutagenesis kit (Stratagene). Additionally, HA-tagged Sufu WT and Sufu mutant S352F were cloned into the pBABE-Puro vector.

Human *Gli1* coding sequence (isoform 1, NM_005269.2) carrying a FLAG tag at the C-terminus was PCR amplified and cloned into the pCMV5 plasmid.

All the constructs were verified by sequencing. The oligonucleotides used for the generation of all the constructs used in this study are available upon request.

Plasmid and siRNA transfections

For plasmid transfection, polyethylenimine (PEI Max, Polysciences Inc.) was used for transfection of HEK293T, X-tremeGENE HP (Roche) for NIH3T3 and HeLa cells and Lipofectamine LTX with *Plus* reagent (Invitrogen) was used for transfection of *Ptch1*^{-/-} and *Sufu*^{-/-} MEFs according to the manufacturer's instructions. For co-immunoprecipitation assay, 48 hours post-transfection, cells were treated with the Nedd8-activating enzyme inhibitor MLN4924 (1 μM, Millenium Pharmaceuticals) and collected after 5 hours.

For siRNA transfection, 30nM of siRNA duplexes were transfected in HeLa, PC3, *Ptch1*^{+/+}, *Ptch1*^{+/-} and *Ptch1*^{-/-} MEFs using Lipofectamine RNAi MAX (Invitrogen) and in DAOY cells using HiPerFect (Qiagen). Next day, a second round of transfection was performed, and the cells were harvested 24 hours after the second transfection. This protocol was used for all cell lines, except DAOY for which one round of transfection was applied and the cells were harvested after 24 hours. The siRNA duplexes used to target human *Fbxl17* transcript (*Fbxl17* siRNA 1 and 2) were described earlier (Tan et al, 2013). To target the expression of human *Sufu* and mouse *Fbxl17* transcripts, we used Ambion[®] Silencer[®] Select Pre-designed siRNA

oligonucleotides (Sufu siRNA 1 [s28521] and Sufu siRNA 2 [s28522]; mFbx117 siRNA 1 [s78415] and mFbx117 siRNA 2 [s78417], respectively, Life Technologies).

For combined DNA and siRNA transfection, HEK293T cells were transfected using Lipofectamine 2000 (Invitrogen) according to the manufacturer's specifications. Plasmids were delivered to the cells along with the siRNA duplexes in the first round of transfection

Lysate production, co-immunoprecipitation and Western blotting

For the production of whole-cell lysates, cells were lysed in lysis buffer (LB) containing 50 mM tris-HCl at pH 7.4, 1mM EDTA, 150 mM NaCl, 5 mM MgCl₂, 0.1% NP-40, 1% glycerol and supplemented with protease and phosphatase inhibitors. After 10 minutes of incubation on ice, the lysates were clarified by centrifugation for 10 minutes in a refrigerated microcentrifuge at 14,000 rpm (revolutions per minute). All the immunoprecipitations involving Flag-tagged proteins were performed as described previously (D'Angiolella et al, 2012). Flag/Myc-tagged Fbx117 co-immunopurified was analysed using liquid chromatography tandem mass spectrometry as described below. For co-immunoprecipitation of HA- or Myc-tagged, the appropriate antibodies were incubated with whole cell lysates for 2 hours at 4°C followed by the addition of Protein G agarose beads (Sigma-Aldrich) and incubation for 2 additional hours. For co-immunoprecipitation of endogenous proteins, the corresponding primary antibodies and whole cell lysates were incubated overnight at 4 °C with rotation. The beads were washed three times with LB and eluted in 2X SDS sample buffer. The samples were boiled for 5 minutes at 90°C prior separation on 4–12% Novex bis-tris gels (Life Technologies). Primary antibodies were diluted at 1:1,000 in blocking solution (5% nonfat dry milk in PBS with 0.1% Tween 20) and

incubated for 1 hour at room temperature. HRP-conjugated secondary antibodies (1:1,000; Life Technologies) or HRP-conjugated Protein A/G (1:5,000; Pierce) were used for protein detection.

Cell fractionation

Ptch1^{-/-} MEFs stably expressing Myc-tagged Fbxl17 were grown to confluence, serum starved in serum-reduced medium for 24 hours and submitted to cell fractionation using standard procedures described previously (Mendez & Stillman, 2000). Western blotting detection of Lamin A/C and GAPDH was performed to assess the purity of the nuclear and cytoplasmic extracts, respectively.

Protein turnover

HeLa cells were transfected with either non-targeting or two different Fbxl17 siRNA duplexes for two consecutive days, and 24 hours later, cells were washed and treated with 50 µg/ml cycloheximide (CHX) to inhibit further protein synthesis. At the end of each time point, cells were harvested, and endogenous Sufu was detected by immunoblot using 3 µg of whole-cell lysate. Sufu mutant S352F along with siRNA duplexes were transfected into NIH3T3 cells and CHX treatment was performed 24 hours after the second round of siRNA transfection when cells reached confluence.

RNA isolation, reverse transcription and real-time quantitative PCR (RT-qPCR)

Total RNA was purified using RNeasy Mini Kit (Qiagen) and complementary DNA was synthesized from 1 µg of total RNA using Oligo(dT) primers and Superscript III reverse transcriptase (Invitrogen) following the manufacturer's specifications. Quantitative RT-PCR was performed using gene-specific primers and

SYBR[®] Green PCR master mix (Life technologies) on a 7500HT Real-time PCR System (Applied Biosystems). Fbx117, GAPDH, Sufu, Gli1 and Bcl2 primer sequences were described previously (Liu et al, 2006; Tan et al, 2013; Yue et al, 2009). All samples were assayed in triplicate and normalized to GAPDH.

Generation of stable cell lines

Myc-tagged Fbx117, HA-tagged Fbx117 and HA-tagged Sufu retroviral plasmids or an empty backbone retrovirus (EV) along with pCMV-Gag-Pol vector and pCMV-VSV-G envelope-encoding vector were used for retrovirus production in HEK293T cells. Twenty four hours post-transfection, the growth medium was changed. Forty-eight hours later, supernatants were harvested and filtered through a 0.45- μ m filter. Stably transduced PC3, DAOY cells *Sufu*^{-/-} and *Ptch*^{-/-} MEFs were generated by retrovirus infection at 1 multiplicity of infection (MOI), in the presence of 8 μ g/ml polybrene, and followed by puromycin selection (1 μ g/ml) for 3 days. Expression of the protein of interest was confirmed by Western blotting.

Immunofluorescence

Ptch^{-/-} MEFs transduced with either Myc-tagged Fbx117 expression construct or an empty vector were seeded on poly-D-lysine coated coverslips and cultured for 72 hours. Cells were fixed for 15 min at room temperature in PBS with 4% formaldehyde, permeabilised with 0.5% Triton X-100 in PBS and blocked using 5% BSA in PBS with 0.1% Triton X-100. Fbx117 was detected using anti-Myc antibody at a dilution of 1:2,000, and endogenous Sufu was stained using goat anti-Sufu antibody at a dilution of 1:100. Primary antibody incubation was performed overnight at 4°C. Secondary antibodies Alexa Flour[®] 488 donkey anti-mouse (1:1,000; Life

Technologies) was incubated for 30 min at room temperature. Nuclei were counterstained using DAPI and the coverslips were mounted with Prolong® Gold antifade reagent (Molecular Probes, Life Technologies). Cells were imaged on a Zeiss Axiovert microscope (63X oil immersion objective lens).

Cell proliferation assay

PC3 and DAOY cells were seeded in 6-well plates and transfected with either non-targeting or two different Fbx117 siRNA duplexes for two consecutive days, and 24 hours later, cells were transferred into 15-cm plates and allowed to grow for 10 days. For standard rescue experiments, Myc-tagged Fbx117 full-length construct was re-introduced in the cells 24 hours after the second round of siRNA. *Sufu*^{-/-} MEFs transduced with an empty backbone retrovirus along with *Sufu*^{-/-} cells stably expressing Sufu WT or Sufu mutant S352F were seeded in 10-cm plates and allowed to grow for 5 days. Cell proliferation rate was assessed by cell counting in three independent experiments. Cell counts corresponding to Fbx117 siRNA-transfected cells were expressed relative to those of non-targeting siRNA, whereas the cell number corresponding to *Sufu*^{-/-} expressing Sufu WT or Sufu S352F were represented relative to the control cell line.

GCPs culture and proliferation assay

Cerebellar GCPs were prepared from 5 old mice as previously described and plated at a density of 8×10^5 cells/cm² on eight-well chamber slides coated with 1 mg/ml poly-L-lysine. For RNA interference, GCPs were transfected with HiPerFect transfection reagent (Qiagen, Hilden, Germany), and for plasmids with Lipofectamine 2000 (Thermo Fisher Scientific, Waltham, MA, USA), according to the

manufacturer's instructions. Cell proliferation was evaluated by BrdU detection (Roche, Welwyn Garden City, UK). Briefly, 24 hours after transfection the BrdU pulse (24 hours) was performed. Cells were then fixed with 4% paraformaldehyde and permeabilized with 0.2% Triton X-100, and BrdU detection was performed according to the manufacturer's instructions. Nuclei were counterstained with Hoechst reagent. At least 500 nuclei were counted in triplicate, and the number of BrdU-positive or BrdU/GFP positive nuclei was recorded (Argenti et al, 2005).

Luciferase reporter gene assay

Sufu^{-/-} MEFs and MEFs stably expressing WT or S352F mutant Sufu were seeded in 6-well plates and co-transfected with 1 µg of the luciferase reporter plasmid 8 X GliBS-luciferase (Sasaki et al, 1997) together with 250 ng of the *Renilla* luciferase pRL-TK reporter (Promega). Cells were serum starved 48 hours post-transfection and Hh stimulation using SAG was initiated 24 hours later. Cells lysis and dual-luciferase measurement were performed 48 hours post-induction using the Dual-Glo luciferase assay system (Promega). All measured luciferase activities were normalized to pRL-TK.

shRNA lentivirus production and Fbx17 knockdown

Endogenous Fbx17 was knocked down using shRNA delivered to cells via a lentiviral system. The shRNA-expressing lentiviruses were generated as previously described (D'Angiolella et al, 2012). Expression arrest pGIPZ lentiviral vectors encoding a non-targeting shRNA (5'-TCTCGCTTGGGCGAGAGTAAG-3') or Fbx17 shRNAs (5'-AGACAAGACCTATCAGTAA-3') were provided by the Target Discovery Institute High Throughput Core (University of Oxford, UK). Transduction

of DAOY cells with either non-targeting or Fbx117 shRNA-expressing lentiviruses was carried out in the presence of 8µg/ml polybrene, followed by selection in growth medium containing 1µg/ml puromycin during 3-4 days.

Immunohistochemistry

All animals were transcardially perfusion-fixed under terminal anaesthesia with 0.9% heparinised saline followed by periodate lysine paraformaldehyde (PLP) containing only 0.025% glutaraldehyde (PLP_{light}) at the end of the experiment (10 week after tumour induction). The brains were post-fixed, cryoprotected, embedded in tissue-tek (Sakura Finetek Europe) and frozen in isopentane at -40°C. Frozen, 10-µm thick, serial sections spanning the tumour in the cerebellum were cut from fixed tissue using a cryostat (Leica CM1900) and mounted onto gelatine-coated slides.

Immunohistochemistry was performed with antibodies against markers of DAOY cells (Vimentin) and proliferation (Ki67). Sections were counter-stained with 0.5% cresyl violet (Sigma Aldrich).

In each group of animals, tumour area per mm² of brain were quantified on four 10-µm-thick sections immediately adjacent to the injection site by drawing around the area of vimentin staining using Aperio ImageScope Software (Leica microsystem). Proliferative index was calculated by determining the percentage of Ki67 positive cells (brown) within the tumour from four brain sections spanning the tumor site.

Appendix Figure legends

Appendix Figure S1

A. **Detected posttranslational modifications of wildtype Sufu after immunopurification and LC-MS/MS analysis.** Blue bars represent detected Sufu derived peptides. S352 is covered with multiple detections and modifications. Phosphorylated S352 was not detected. S346, S349 and T353 were found phosphorylated and the sites confirmed by presence of diagnostic fragment ions in the MS/MS spectra.

B. **Sufu degradation by Fbx17 allows Gli dissociation for Hedgehog signaling activation.** Detection of Fbx17 mRNA levels in *Ptch1*^{-/-} MEFs transfected with non-targeting siRNA (Control) or two siRNAs against Fbx17.

Appendix Figure S2. Fbx17 mediated degradation of Sufu regulates Hh signaling and proliferation in prostate cancer cell (PC3).

A. Gli1 mRNA levels after transfection of PC3 cells with a non-targeting siRNA (Control) or two siRNAs to Fbx17 (1) and (2). (mean ± SEM from 3 independent experiments, **p<0.005).

B. Gli1 mRNA levels in PC3 cells after transfection with an Empty Vector (EV) or a vector expressing Myc-Fbx17. (mean ± SEM from 3 independent experiments, **p<0.005).

C. Cell proliferation of PC3 cells upon Fbx17 depletion using two different siRNAs or upon reintroduction of a Myc-tagged Fbx17 construct in Fbx17-depleted PC3 cells (mean ± SEM from 3 independent experiments, *p<0.05; ***p<0.0005).

D. Sufu protein levels in PC3 cells treated as in C. Representative image of three independent experiments is shown.

E. Relative abundance of Sufu protein in PC3 cells treated as in C (mean \pm SEM from 3 independent experiments, * p <0.05; ** p <0.005).

F. Quantification of Fbx17 mRNA levels in PC3 cells upon transfection with a non-targeting siRNA (Control) or two siRNAs to Fbx17 (1) and (2).

Appendix Figure S3. Fbx17 mediated degradation of Sufu regulates proliferation of prostate cancer cells (PC3)

A. Cell proliferation of PC3 cells transfected with non-targeting siRNA (Control), siRNA against Fbx17 or a combination of siRNA targeting Fbx17 and Sufu. (mean \pm SEM from 3 independent experiments, *** p <0.0005; NS, non-significant).

B. Detection of Sufu protein levels treated as in A. Representative image of three independent experiments is shown.

C. Relative abundance of Sufu protein in PC3 cells treated as in A (mean \pm SEM from 3 independent experiments, * p <0.05).

D. Quantification of Fbx17 mRNA levels in PC3 cells upon Fbx17 depletion using either a non-targeting siRNA (control) or two siRNAs to Fbx17 (1) and (2) (mean \pm SEM from 3 independent experiments, *** p <0.0005).

Appendix Figure S4. Fbx17 mediated degradation of Sufu regulates proliferation of medulloblastoma cells (DAOY)

A. Relative abundance of Sufu protein in DAOY cells treated as in Fig 5A (mean \pm SEM from 3 independent experiments, * p <0.05; ** p <0.005; *** p <0.05).

B. Relative abundance of Sufu protein in DAOY cells treated as in Fig 5D (mean \pm SEM from 3 independent experiments, ** p <0.005; *** p <0.0005).

Appendix Figure S5. T1-weighted MRI assessing medulloblastoma tumour growth upon Fbx117 silencing

A. Relative abundance of Sufu protein levels in DAOY cells transfected with Control shRNA or shRNA against Fbx117 (mean \pm SEM from 3 independent experiments, *** p <0.0005).

B. T₁-weighted magnetic resonance representative images taken at 10 weeks showing vessel permeability in rats injected with DAOY cells transfected with control shRNA or shRNA against Fbx117. Scale bar: 5mm.

C. Bar chart showing gadolinium-enhanced T₁ hyperintensity (a surrogate marker of tumour vessel permeability) at 10 weeks in both groups. Animals were injected with DAOY cells stably expressing either control shRNA or shRNA against Fbx117 (10,000 cells/1 μ L). (mean \pm SEM; n=5; two-way ANOVA, followed by unpaired t-test, * p <0.05, ** p <0.01).

References

Argenti B, Gallo R, Di Marcotullio L, Ferretti E, Napolitano M, Canterini S, De Smaele E, Greco A, Fiorenza MT, Maroder M, Screpanti I, Alesse E, Gulino A (2005) Hedgehog antagonist REN(KCTD11) regulates proliferation and apoptosis of developing granule cell progenitors. *The Journal of neuroscience : the official journal of the Society for Neuroscience* **25**: 8338-8346

D'Angiolella V, Donato V, Forrester FM, Jeong YT, Pellacani C, Kudo Y, Saraf A, Florens L, Washburn MP, Pagano M (2012) Cyclin F-mediated degradation of ribonucleotide reductase M2 controls genome integrity and DNA repair. *Cell* **149**: 1023-1034

Liu G, Yuan X, Zeng Z, Tunici P, Ng H, Abdulkadir IR, Lu L, Irvin D, Black KL, Yu JS (2006) Analysis of gene expression and chemoresistance of CD133+ cancer stem cells in glioblastoma. *Molecular cancer* **5**: 67

Mendez J, Stillman B (2000) Chromatin association of human origin recognition complex, cdc6, and minichromosome maintenance proteins during the cell cycle: assembly of prereplication complexes in late mitosis. *Molecular and cellular biology* **20**: 8602-8612

Sasaki H, Hui C, Nakafuku M, Kondoh H (1997) A binding site for Gli proteins is essential for HNF-3beta floor plate enhancer activity in transgenics and can respond to Shh in vitro. *Development* **124**: 1313-1322

Tan MK, Lim HJ, Bennett EJ, Shi Y, Harper JW (2013) Parallel SCF adaptor capture proteomics reveals a role for SCFFBXL17 in NRF2 activation via BACH1 repressor turnover. *Mol Cell* **52**: 9-24

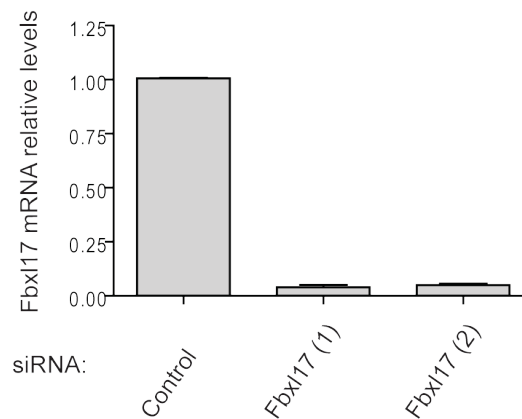
Yue S, Chen Y, Cheng SY (2009) Hedgehog signaling promotes the degradation of tumor suppressor Sufu through the ubiquitin-proteasome pathway. *Oncogene* **28**: 492-499

Appendix Figure S1

A

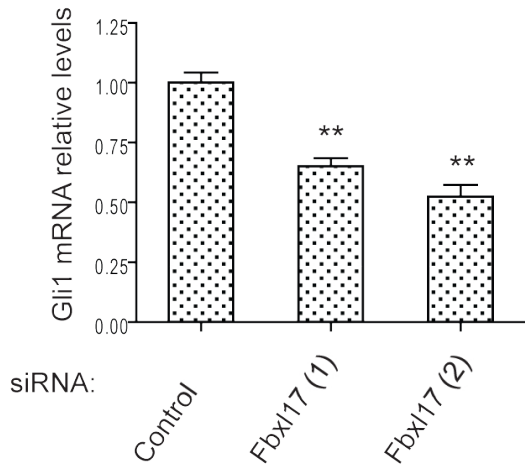


B

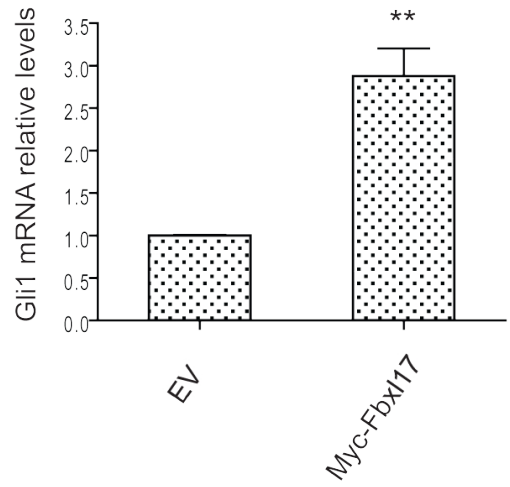


Appendix Figure S2

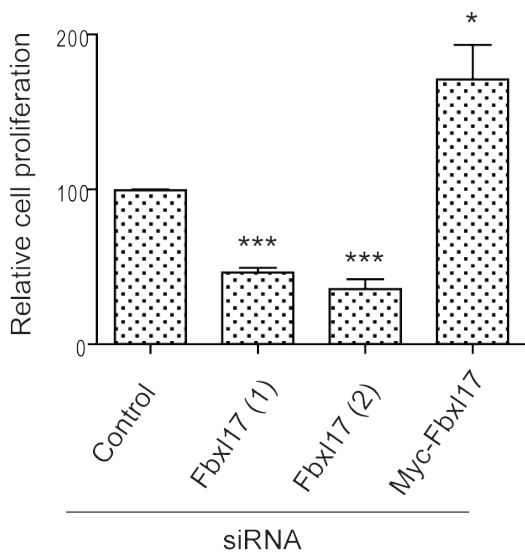
A



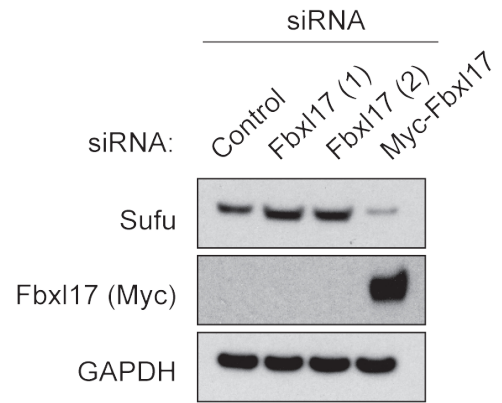
B



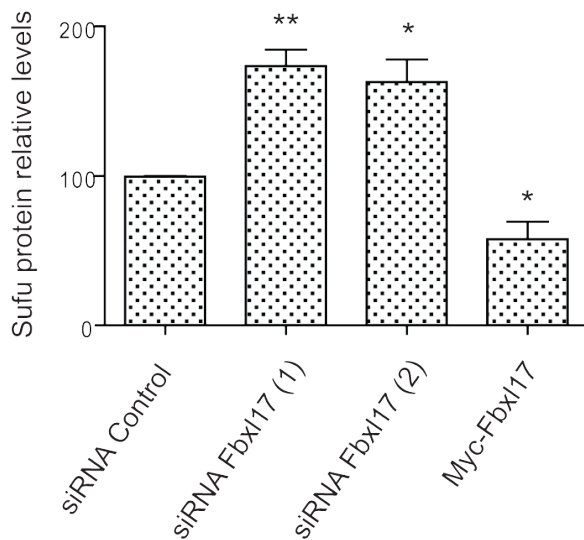
C



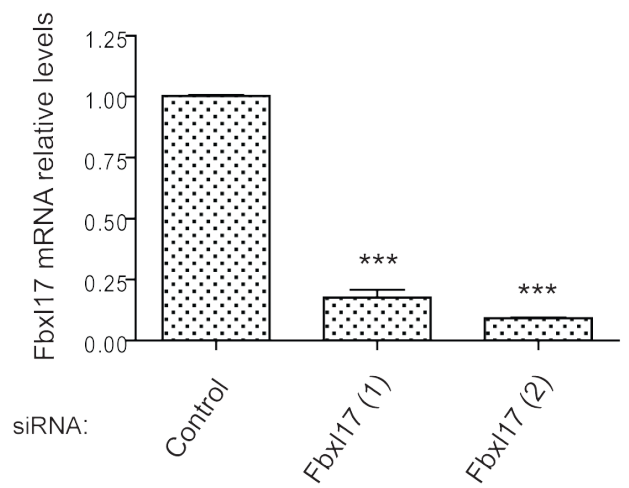
D



E

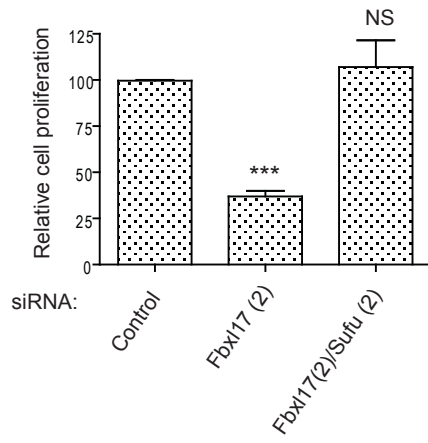


F

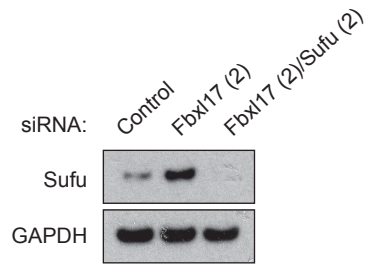


Appendix Figure S3

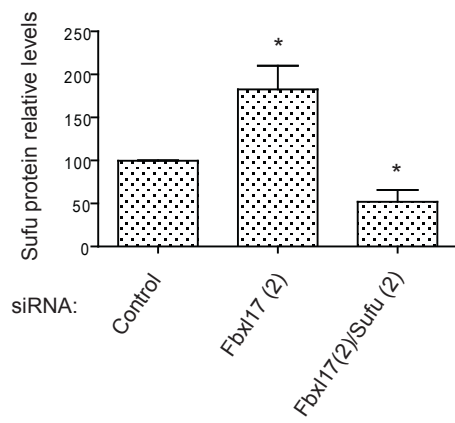
A



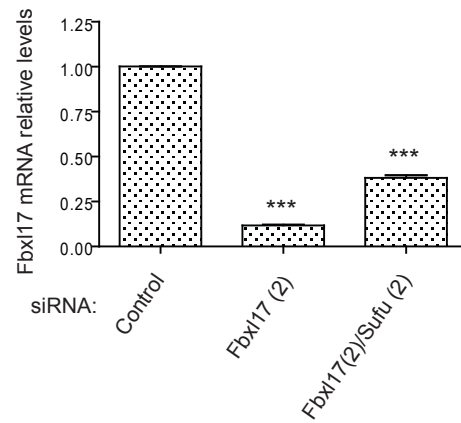
B



C

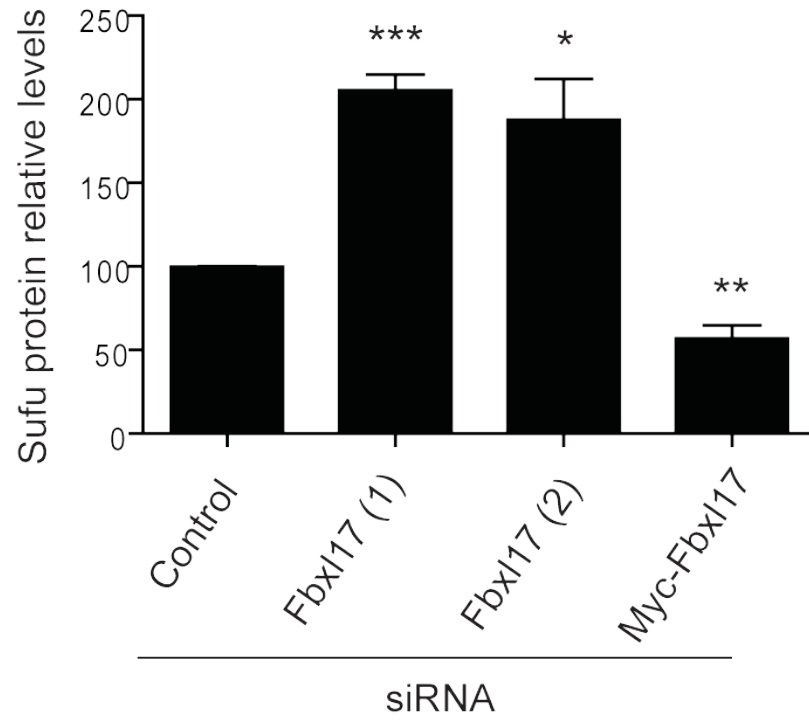


D

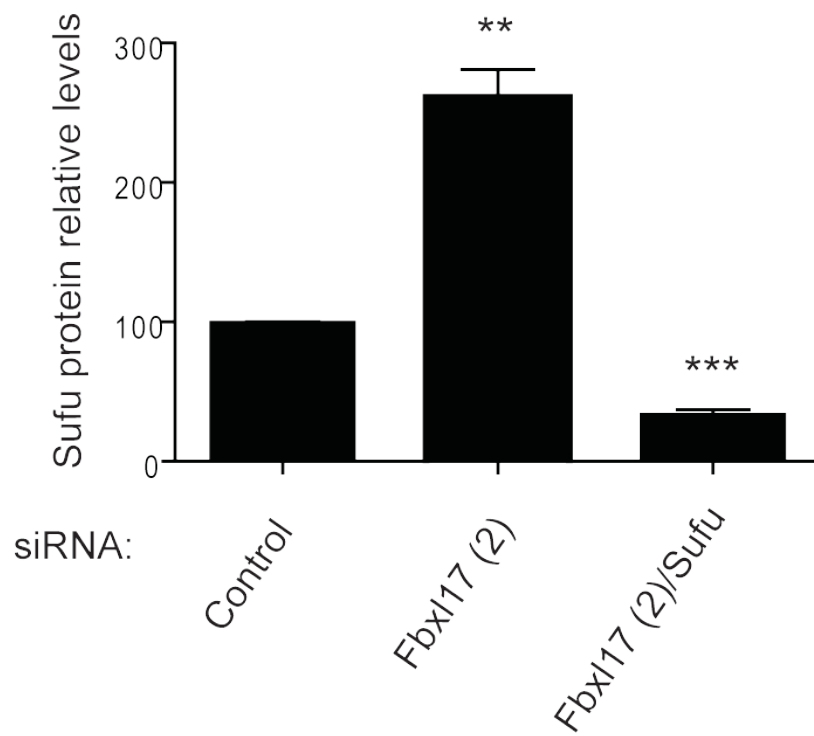


Appendix Figure S4

A

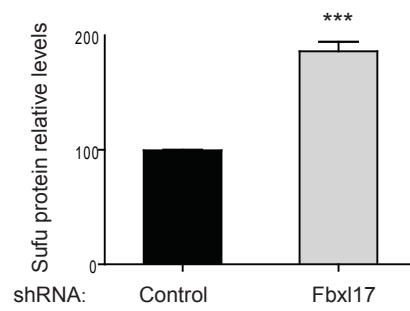


B

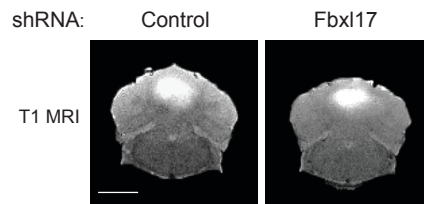


Appendix Figure S5

A



B



C

